

Notice: This material may be protected by Copyright Law (Title 17 U.S.C.).

PRESSURE SWING ADSORPTION: EXPERIMENTAL ANALYSIS
OF THE METHOD OF CHARACTERISTICS THEORETICAL MODEL

A Thesis

Presented in Partial Fulfillment of the Requirements
for the Degree Master of Science

by

John C. Kayser, B.Ch.E.

The Ohio State University

1985

Approved by

Kent S. Knobell
Adviser

Department of
Chemical Engineering

Copyright © 1985
by John C. Kayser.

ACKNOWLEDGEMENTS

I would like to express my thanks to Dr. Kent S. Knaebel for his help in every aspect of this study. His theoretical work formed a framework for the study and his experimental guidance was indispensable.

I am grateful to the Air Force Systems Command, the Air Force Office of Scientific Research and the Southeastern Center for Electrical Engineering Education for sponsoring this work. Special thanks are extended to the U.S. Air Force School of Aerospace Medicine, Brooks A.F.B., Texas, for providing facilities and support so this work could be conducted in an efficient manner. In particular, the support of Dr. Kenneth G. Ikels and Mr. Clarence Theis was invaluable.

As a result of government sponsorship the following acknowledgement is in order. This research was sponsored by the Air Force Office of Scientific Research/AFSR United States Air Force, under Contract F49620-82-C-0035. The United States Government is authorized to reproduce and distribute reprints for governmental purposes notwithstanding any copyright notation hereon.

TABLE OF CONTENTS

	Page
TABLE OF FIGURES	iv
TABLE OF TABLES	v
SUMMARY	vi
I. INTRODUCTION	1
II. THEORY	4
III. EXPERIMENTAL METHODS AND DATA	14
IV. CONCLUSIONS AND RECOMMENDATIONS	50
NOMENCLATURE	52
REFERENCES	55
APPENDIX	56

TABLE OF FIGURES

Figure	Page
1 Six-Step, Two-Bed PSA Cycle	6
2 Four Actual Steps of a PSA Bed in the PSA Cycle	7
3 Void Fraction Apparatus	17
4 Equilibrium Isotherms of N ₂ and O ₂ on 5A at 30 ⁰ C	20
5 Equilibrium Isotherms of N ₂ and O ₂ on 5A at 45 ⁰ C	21
6 Equilibrium Isotherms of N ₂ and O ₂ on 5A at 60 ⁰ C	22
7 Adsorption Equilibrium Apparatus	23
8 Diagram of Breakthrough Unit	27
9 Actual and Ideal Breakthrough Curves	30
10 Two-Bed PSA Process Diagram	32
11 Pressure-vs-Time For an Ideal Six-Step Cycle	34
12 Ave. Bed Pressure-vs-Time for Actual Six-Step Cycle	36
13 Ideal-vs-Actual Pressure Swing Cycles	39
14 Oxygen Recovery at 45 ⁰ C	43
15 Nitrogen Breakthrough at 30 ⁰ C	46

TABLE OF TABLES

Table	Page
1 Void Fraction Measurements on Zeolite 5A	18
2 Linear Regression of Equilibrium Data	24
3 Equilibrium Isotherms from Breakthrough Experiments	28
4 Solenoid Valve Positions for Six-Step Cycle	35
5 PSA Recovery Data, O ₂ + Ar from Air	44
6 Typical Cycle Times	45
7 Nitrogen Breakthrough at 30°C	47

SUMMARY

The pressure swing adsorption (PSA) theory of Knaebel and Hill [8] is experimentally tested under conditions favorable to the assumptions and constraints of the theoretical model. The major assumptions of the theory are local equilibrium and negligible dissipative effects while the primary constraints are linear, uncoupled isotherms and binary feed gas. The binary mixture studied is nitrogen-oxygen while the adsorbent used in all experiments is zeolite molecular sieve 5A. To test the theory the following experimental studies are performed:

1. void fraction determination
2. equilibrium isotherm measurement
3. breakthrough experiments
4. two-bed, six-step PSA process operation with pressurization with product.

The void fraction measurement is necessary since it is an input parameter in all the other experiments. Determination of the void fraction enables calculation of the particle density which is needed in the equilibrium isotherm measurements. The void fraction is an important parameter in the equations of the theory of Knaebel and Hill [8].

The equilibrium isotherm measurements are performed to identify the regions in which the isotherms are linear. Nitrogen and oxygen adsorption is measured using the volumetric technique at 30⁰C, 45⁰C, and 60⁰C up to pressures of 3500 mmHg. The isotherms of nitrogen are found to be approximately linear at 45⁰C and 60⁰C up to 3500 mmHg. Oxygen isotherms are linear for the entire range of temperatures and pressures studied. The slopes of the linear isotherms are used as input parameters in the theory of the PSA process and are used for comparison with values predicted using the breakthrough experiments.

Application of the theory to breakthrough experiments enables calculation of the slopes of linear equilibrium isotherms with an average absolute percent difference from the actual measurements of 5.4%. The theory is successful in six different determinations of linear isotherms from 3 psia to 45 psia and 20⁰C to 60⁰C. The results support the validity of the theory for the conditions of the experiments and indicate that the breakthrough experiment is an efficient technique for evaluating isotherms.

The PSA process experiments support the theory also. The theory predicts the complete clean up of the light component and also the recovery of the light component as a function of the pressure ratio, feed composition, and temperature of the process. For the separation of oxygen and argon (which constitute the light component) from nitrogen (the heavy component) the average purity of light product is 99.6%_{vol.} and never less than 99.2%_{vol.}. The

recovery of the light component is predicted with an average absolute error of 7.1% relative to actual experimental values measured over a wide range of pressure ratios (from 6.5 to 840) at 45°C and 60°C.

As noted, the theory is tested under conditions supportive of the assumptions and constraints given in the derivation. Relaxing the assumptions and constraints by performing experiments under different conditions is a good place to begin further work. For example, the local equilibrium assumption is supported here by slowly cycling the process (i.e., low throughput of feed gas); the effect of faster cycling needs to be investigated. Several other recommendations for further experimentation are given.

CHAPTER I

INTRODUCTION

Pressure Swing Adsorption (PSA) is a cyclic process used for the separation of gaseous mixtures. PSA processes can be economically built and operated for large or small scale throughputs of feed gas and are capable of producing pure product. Consequently, PSA processes are finding broad applications industrially. Production of oxygen [1,2,3], hydrogen purification [4,5], and air drying [6,7] are a few examples.

Industrial application of PSA processes has proceeded without a theoretical framework. Few theoretical analyses of PSA processes have appeared in the open literature. In addition, the published theories have not been experimentally confirmed.

Knaebel and Hill [8] recently developed a theory of PSA processes which is a significant extension of earlier theoretical models. Their analysis is for the purification of the light component* of a binary feed gas of arbitrary composition. The preceding theories [9,10] are limited to the purification of the

* The light component refers to the species of the binary which is less preferentially adsorbed. The light component, by convention, is labeled as species B. The heavy component, which is preferentially adsorbed, is species A.

light component from a binary feed gas containing only a dilute heavy component. The assumption of local equilibrium and the constraint of linear adsorption equilibrium isotherms are common to the theories [8,9,10] and limit their applicability. Nevertheless, if the theory of Knaebel and Hill [8]* is valid under conditions which support the assumptions and constraints made in the derivation, then the theoretical model represents a significant step in the development of a theoretical framework of PSA. Furthermore, from a practical perspective, the model could be quite useful in the design and performance testing of PSA processes.

The primary scope of this work is to experimentally test the theoretical model derived by Knaebel and Hill [8]. Using the theory the following experimental objectives are defined.

1. To predict the slopes of linear adsorption equilibrium isotherms by applying the theory to dynamic breakthrough experiments.
2. To construct and operate a PSA process in order to compare the actual performance of the process with the predictions of the theory.

The order of the remaining chapters is designed to clarify and meet the objectives stated above. In the next chapter, the theory pertinent to this experimental work is presented. Chapter III summarizes the experimental work and results. In Chapter IV,

* Throughout the text the phrases "the model" and "the theory" refer to the equations derived in Reference [8] including assumptions and constraints made in the derivation.

conclusions concerning the theory and the experimental results are consolidated. In addition, recommendations are made primarily directed towards possible future experimentation.

CHAPTER II

THEORY

A. Process Description

PSA works on the basis of preferential adsorption of one component of a mixture on an adsorbent solid. An adsorbed component can be partially removed from the solid by decreasing the pressure of the gas around the solid. Hence, by "swinging the pressure" from high to low a strongly adsorbed component can be trapped via adsorption at high pressure and released via desorption at low pressure.

Many PSA process configurations are possible. One-column and two-column processes are the most common. The two-column process, as opposed to the one-column process, is capable of producing pure product and is therefore of considerable interest. Attention will be restricted here to the two-column process. Knaebel and Hill [8] restrict their analysis to the two-column process also.*

There are several operational variations of the two-column process. The arrangement of the process flow streams and differing

* The equations derived in Reference [8] are, however, applicable (in part) to a single column and easily extended to multiple column processes.

number of cycle steps distinguish each variation. Miller [11] discusses several two-column processes. This work is restricted to the pressurization with product, six-step process shown schematically in Figure 1. The arrangement is an excellent one for testing the model for several reasons. For one, the model equations are algebraic results of an exact solution to continuity (i.e. numerical calculations are unnecessary). More importantly, the six-step cycle shown can be constructed so that steady state feed and product rates can be attained in the laboratory resulting in simplified and accurate mass balance accounting. The general model [8], it should be noted, is not restricted to the process given in Figure 1. For example, the model can be applied to a process otherwise identical to Figure 1 except for a pressurization step using feed gas.

Each column in the six-step cycle of Figure 1 experiences only four actual steps: high pressure feed, blowdown to low pressure, purge at low pressure, and pressurization (refer to Figure 2). The theoretical analysis of the four actual steps experienced by a single column is sufficient to model the entire two-column process.

B. Analysis of the PSA Cycle

Using the method of characteristics to solve the continuity equation, Knaebel and Hill [8] developed equations to analyze the four steps in Figure 2. The derivation is involved and not

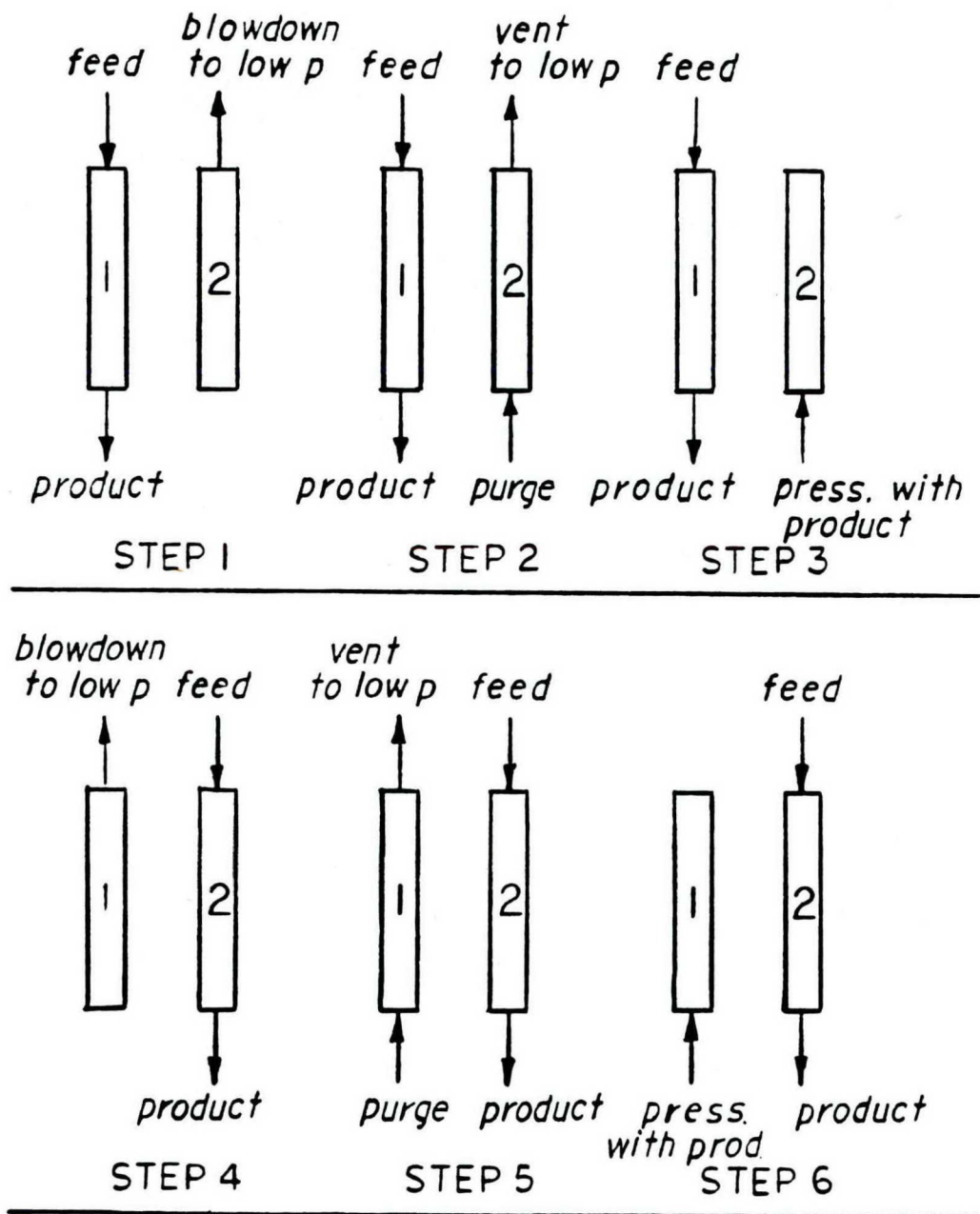


FIGURE 1: SIX-STEP, TWO-BED PSA CYCLE

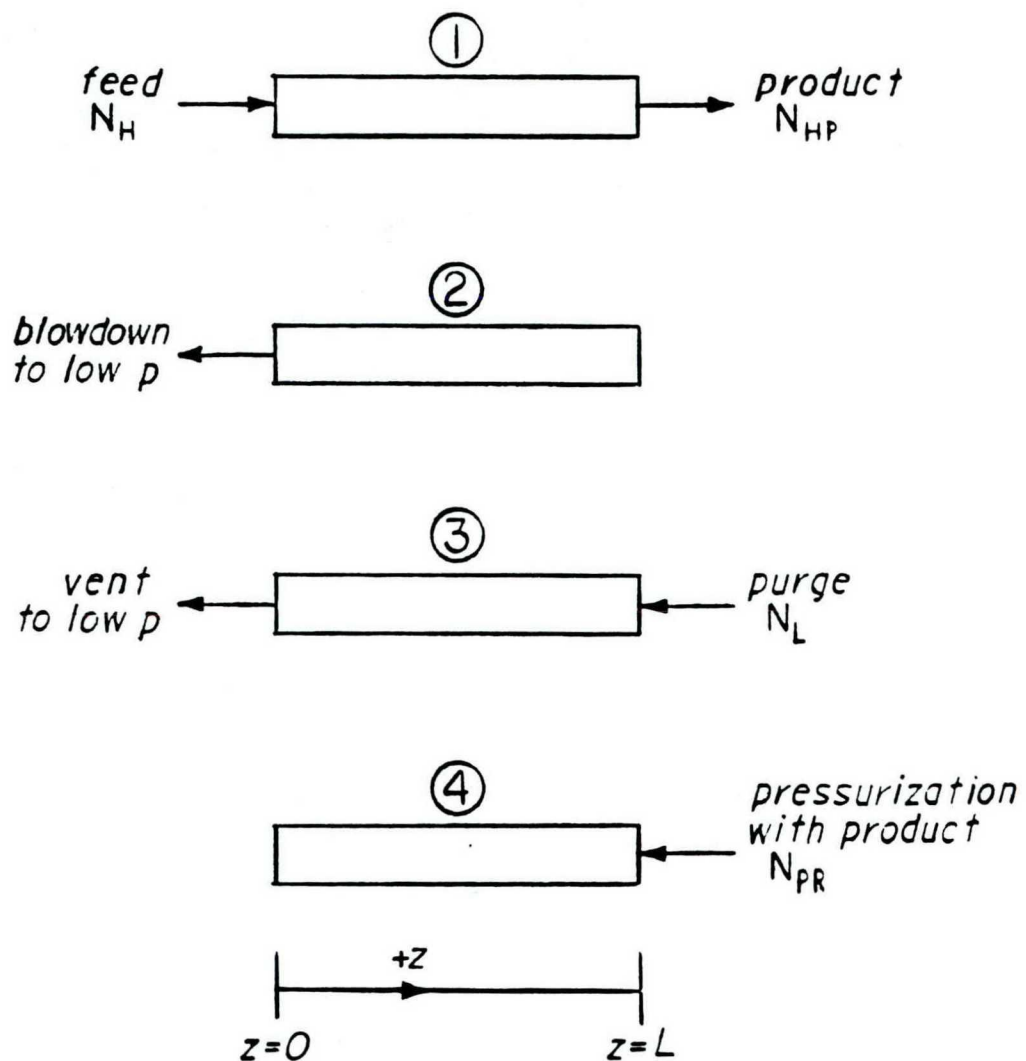


FIGURE 2: FOUR ACTUAL STEPS OF A BED IN
THE PSA CYCLE OF FIGURE 1

presented here. The relevant theoretical information is summarized in this section using the following format.

1. The Assumptions and Constraints
2. General Comments on the Theoretical Behavior of the PSA Cycle
3. Pertinent Theoretical Equations and Comments

The Assumptions and Constraints*

1. Binary gas mixture.
2. Local equilibrium between the gas and solid phases.
3. Linear, uncoupled adsorption equilibrium isotherms.
4. Negligible axial dispersion.
5. Negligible axial pressure gradients. Constant pressure during feed and purge steps.
6. Isothermal operation.
7. Ideal gas behavior.
8. No radial dependence in velocity or composition.
9. Identical columns: identical lengths, cross sectional areas, and interstitial void fractions.
10. Complete purification of the light component using the least possible amount of adsorbent.

* Discussed in the next chapter while only listed here.

General Comments on the Theoretical Behavior of the PSA Cycle

1. The number of moles entering and exiting a given column for each cycle step is independent of flow rate and cycle time. This is a direct result of the assumptions and constraints. As a consequence, the global modeling of the PSA cycle is basically an accounting of the moles entering and/or exiting a column during each process step.
2. The theory predicts the cycle times for the feed and purge steps given the input flow rates, pressure, bed porosity and volume, and equilibrium isotherm information. While flow rate and cycle time do not affect the step by step molar balance they are simply related by the following relation written in particular for the high pressure feed step (at constant T and P).

$$\frac{\text{Moles}}{\text{Feed Step}} = \frac{\text{Cycle Time}}{\text{Feed Step}} \frac{\text{Moles}}{\text{Time}} = \text{Constant}$$

3. One of the most important conclusions of the method of characteristics solution is the prediction of composition shock-waves and composition simple-waves. The former is predicted to occur when gas enriched in A enters a bed dilute in A. Thus, a positive square wave change of the composition of A in a stream entering a bed is maintained along the bed and the effluent gas composition eventually undergoes a square wave or shock change. The feed step of the PSA cycle represents conditions which exhibit the composition shock-wave phenomenon. The feed cycle time is the time required for the composition shock to reach the end of the packed

bed, thus using the adsorbent entirely. The latter case of a simple-wave occurs when a gas enriched in B enters a bed dilute in B. The purge step of the PSA cycle represents conditions in which a composition simple-wave is generated. The important characteristic of the simple-wave is that a positive square wave change in the composition of component B in a stream entering a bed becomes diffuse such that the effluent composition of B only gradually approaches in time the composition of the influent stream. The time that it takes B to entirely purge a bed is the time it takes for the effluent gas composition to equal the influent gas composition.

4. Coincident with the composition shock-wave is a velocity square wave. The influent stream is travelling at a greater velocity than the fluid downstream of the shock due to positive accumulation of gas in the adsorbent occurring at the composition shock front. Thus, during the feed step the product velocity is less than the feed velocity until the composition shock reaches the effluent end of the bed, at which time the velocity instantaneously increases to the feed velocity.

5. Perhaps the most important aspect of the PSA process is the composition shock phenomenon which occurs during the high pressure feed step. The composition shock is the focal point of the separation since the high pressure feed step generates the pure light component which is distributed for product, purge, and pressurization. In theory the composition shock is formed

immediately at the inlet of the bed. Consequently, for a fixed molar feed rate and identical pressures and temperatures, a small volume bed acting with short cycle times produces identical product flow as a larger volume bed operating at longer cycle times.

6. Finally, it should be remembered that the comments above and the equations which follow are contingent upon the validity of the assumptions and constraints listed earlier. Additional comments are given with the equations presented below.

Pertinent Theoretical Equations and Comments

The theory predicts the cycle times of the high pressure feed and low pressure purge steps as follows:

$$t_H = \frac{L}{\beta_A u_H} \quad [1]$$

and

$$t_L = \frac{-L}{\beta_A u_L} \quad [2]$$

with

$$\beta_i = \frac{1}{1 + \left(\frac{1 - \epsilon}{\epsilon}\right) k_i} \quad [3]$$

The negative sign appears in equation [2] as a result of the sign convention in Figure 2.

A very important measure of the effectiveness of a PSA process is the recovery of light component. It is defined as the net light component product divided by the light component feed and is given by the equation

$$R_{TH} = \frac{N_{HP} - N_L - N_{PR}}{(1 - Y_F) N_H} . \quad [4]$$

The theory provides the following relations to account for the terms given in Equation [4].

$$N_{HP} = \frac{\epsilon A_{cs} L}{RgT} \frac{[1 + (\beta - 1) Y_F] P_H}{\beta_A} \quad [5]$$

$$N_L = \frac{\epsilon A_{cs} L}{RgT} \frac{P_L}{\beta_A} \quad [6]$$

$$N_{PR} = \frac{\epsilon A_{cs} L}{RgT} \frac{P_L (\rho - 1)}{\beta_B} \quad [7]$$

$$N_H = \frac{\epsilon A_{cs} L}{RgT} \frac{P_H}{\beta_A} \quad [8]$$

Substituting Equations [5] - [8] into Equation [4] yields

$$R_{TH} = (1 - \beta) \left(1 - \frac{1}{\rho(1 - Y_F)} \right) \quad [9]$$

where $\beta = \frac{\beta_A}{\beta_B}$ [10]

and $\rho = \frac{P_H}{P_L}$ [11]

The results of the analysis of Knaebel and Hill [8] for the case of pressurization with product are compactly stated by Equation [9]. The term β is a separation factor having magnitude between zero and one. Small values of β correspond to large separability of the components and greater recovery. Large values of β indicate the opposite. The equation indicates the term $\rho(1 - Y_F)$ must be greater than unity before a positive recovery of pure product resulting from complete adsorbent utilization is possible. For the usual case of a fixed composition feed gas, Equation [9] predicts that a certain pressure ratio must be exceeded to recover pure light component product with complete adsorbent utilization. Finally, the maximum theoretical recovery is $(1 - \beta)$ which occurs in the limit of an infinite pressure ratio.

Equations [1] and [9] are two important theoretical results. The experimental work given in the next chapter is concerned primarily with the accuracy of these two equations.

CHAPTER III

EXPERIMENTAL METHODS AND DATA

Prior to experimentation the selection of a binary gaseous mixture and adsorbent capable of separating the species is necessary. The production of oxygen from air is of considerable interest in the PSA field. As a result, the binary mixture of nitrogen and oxygen is studied here.* The gases used and their purities are given for each experiment. Zeolite molecular sieve 5A is used exclusively in all experiments.** Normal procedures are employed to regenerate or activate the molecular sieve (see Appendix).

Evaluation of the accuracy of Equations [1] and [9] allows the two objectives noted in the Introduction to be addressed. Before experiments can be performed which directly involve Equations [1] and [9] several factors must be considered. Evaluations of the physical properties of void fraction, ϵ , and equilibrium adsorption

* Air, which contains ~1% vol. Ar, is used as the feed gas in the PSA process experiments. The effect of the Ar is discussed in the PSA experimental section.

** Union Carbide Corp. Lot. No. 935583080192, 20X40 MESH (~0.01" - 0.02" diameter), medical grade, 20%_{wt.} inert clay binder.

isotherm slopes, K_A and K_B , are necessary. The chapter is divided into two sections to clarify the experimental approach and methods. The topic of the first section is physical property measurements while the second section considers the experimental testing of Equations [1] and [9]. Both sections include an ongoing discussion of the decisions made during experiments to support the assumptions and constraints of the theory. Detailed experimental procedures, data, and calculations are summarized in the Appendix. An equipment summary is also given in the Appendix.

A. Physical Property Measurement

1. Void Fraction Determination

An important parameter in the analysis of flow through packed beds is the void fraction. Simultaneously measuring the void fraction and the bulk density allows calculation of the particle density by the following equation:

$$\rho_p = \frac{\rho_B}{(1 - \epsilon)} \quad , \quad [12]$$

The particle density is a constant for a particular adsorbent, and once it is known, the void fraction can be calculated for any packed bed given the bulk density.

The experimental determination of the void fraction and bulk density, and thus the particle density, is performed using the apparatus in Figure 3. The glass column is packed with molecular sieve 5A followed by the displacement of the void fraction of the bed with a suitable liquid. Knowledge of the pertinent volumes and weight of solids enables calculation of the void fraction. Cyclohexane is used as a displacement fluid since its large molecular diameter indicates that it cannot enter the crystal cages of zeolite 5A. The void fraction is therefore measured as all the voids outside the zeolite crystal lattice divided by the total bed volume. The definition should be equivalent to the fluid mechanical definition as required for use in the theory. To test the hypothesis that cyclohexane is excluded from the zeolite crystal, n-octadecane ($n\text{-C}_{18}\text{H}_{38}$) is used in the identical experiment. It is reasonable to assume that n-octadecane cannot significantly penetrate the zeolite crystal lattice. Table 1 summarizes the results of the void fraction experiments. As the data in Table 1 indicate, a statistically equal void fraction is determined with n-octadecane as with cyclohexane for molecular sieve 5A.

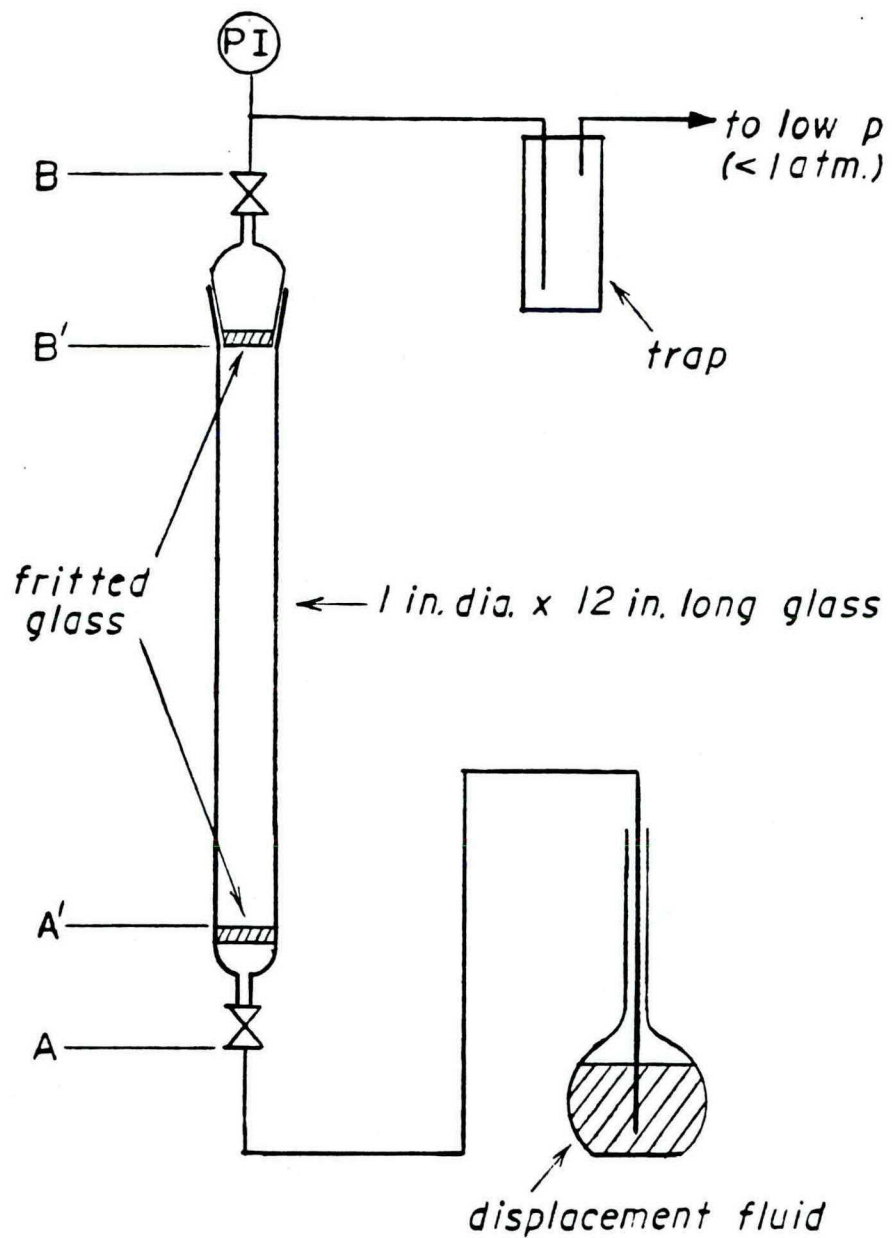


FIGURE 3: VOID FRACTION APPARATUS

Table 1: Void Fraction Measurements on Zeolite 5A

Run	Liquid	ϵ
1	C ₆ H ₁₂	0.492
2	C ₆ H ₁₂	0.477
3	C ₆ H ₁₂	0.463
4	C ₆ H ₁₂	0.476
(Runs 1-4) $\bar{\epsilon} = 0.477 \pm 0.012$		
5	n-C ₁₈ H ₃₈	0.481
(Runs 1-5) $\bar{\epsilon} = 0.478 \pm 0.010$		
$\bar{\rho}_B = 0.810 \pm 0.002 \text{ gm/cc}$		
$\bar{\rho}_P = 1.552 \pm 0.030 \text{ gm/cc}$		

2. Equilibrium Isotherm Measurements

The motives for measuring equilibrium isotherms in this study are to determine the temperatures and pressures where the isotherms are approximately linear and to quantify the adsorption (i.e., K_i) in the linear regions. No attempt is made to theoretically quantify or model the adsorption behavior. In general, the theoretical constraint of linear, uncoupled isotherms is favored at high temperatures and low pressures.

It has been shown that at 24°C oxygen exhibits linear isotherm behavior up to 4000 mmHg while nitrogen adsorption is approximately

linear only to 150 mmHg [11]. In order to study the theory at higher pressures than 150 mmHg it is necessary to ensure that nitrogen adsorption is linear at higher pressures. Consequently, the measurement of adsorption isotherms at elevated temperatures is necessary.

Uncoupled isotherms, which means the adsorption of each component is only dependent on its own partial pressure, has been shown to be a good assumption for the nitrogen-oxygen binary on molecular sieve 5A at 24°C and partial pressures up to at least 2000 mmHg [11]. Coupling is assumed negligible in this study which is reasonable since the temperatures employed are even greater than 24°C. As a result, only pure component isotherm measurements are necessary.

Nitrogen and oxygen isotherms measured at 30°C, 45°C, and 60°C are presented in Figures 4, 5, and 6. Table 2 is a summary of the linear regression performed on the data and the slopes are drawn in Figures 4, 5, and 6. The raw data is tabulated in the Appendix. The apparatus constructed to perform the measurement is shown in Figure 7. The measurement procedure involves the addition of a known amount of gas to bomb A followed by the distribution of the gas in bombs A and B where bomb B contains a known weight of zeolite. Given the particle density, volumes of the apparatus, and the equilibrium pressure and temperature the isotherms can be determined. It is worth noting that the measurement of the adsorption isotherm is dependent upon the value of the particle

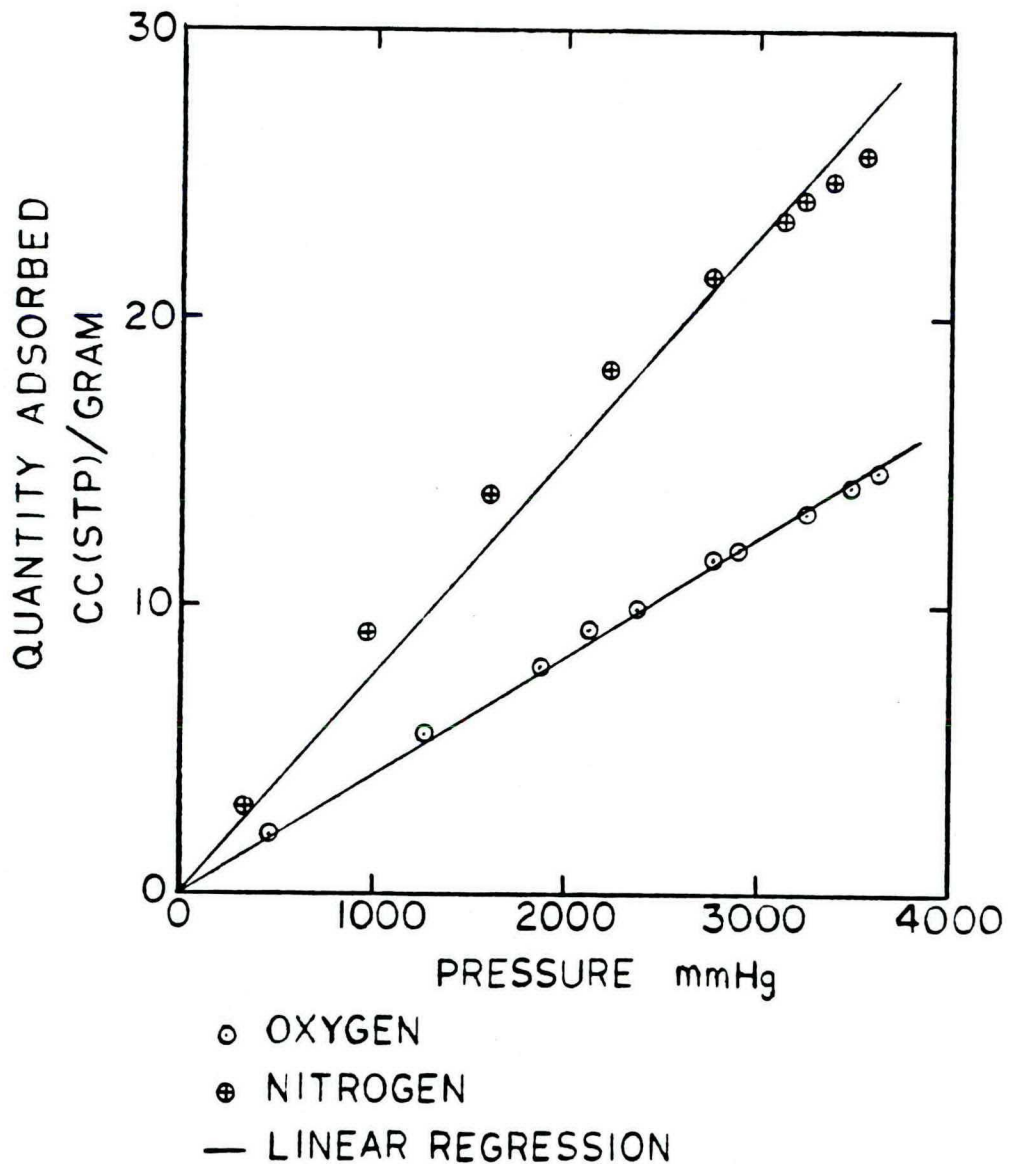


FIGURE 4: EQUILIBRIUM ISOTHERMS OF
N₂ AND O₂ ON 5A AT 30°C

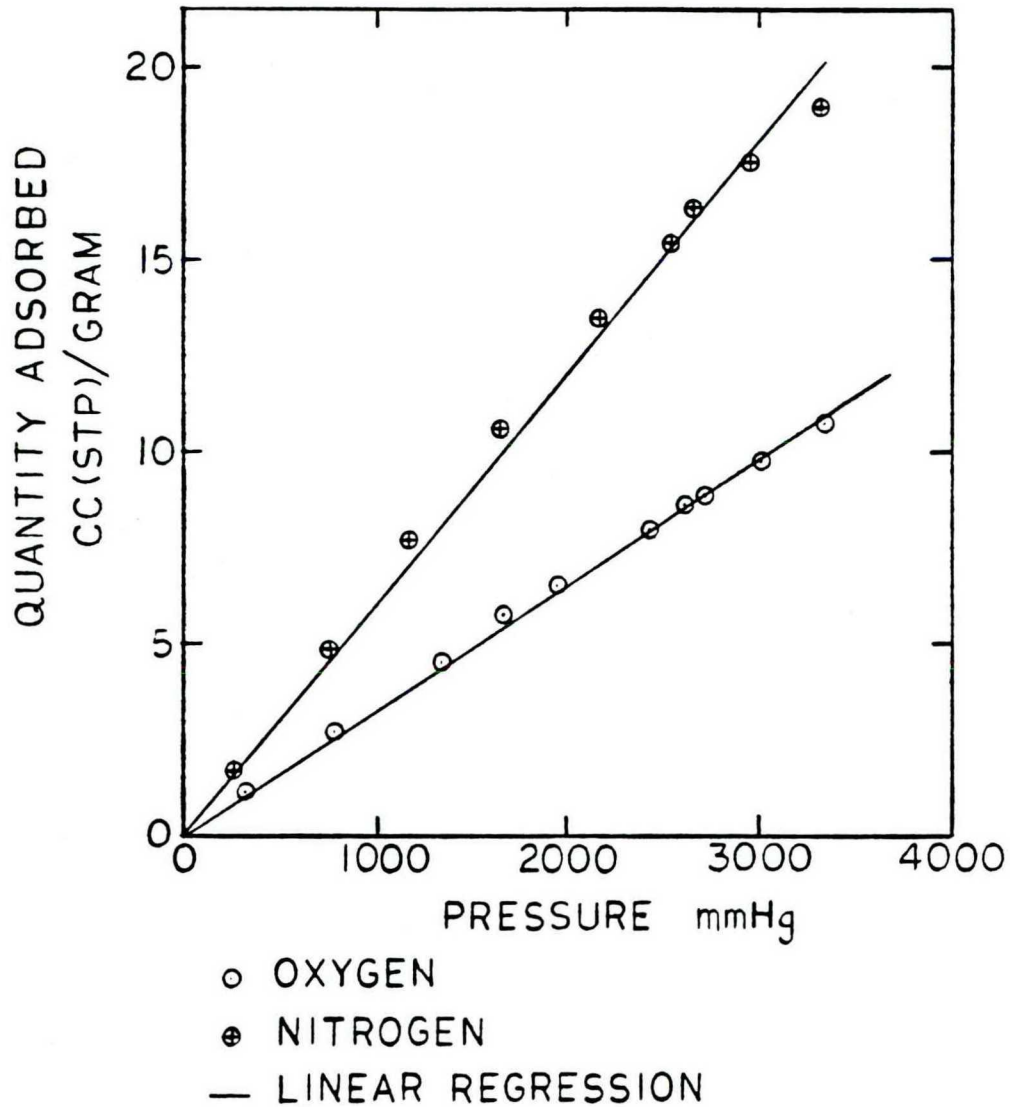


FIGURE 5: EQUILIBRIUM ISOTHERMS OF
 N_2 AND O_2 ON 5A AT $45^\circ C$

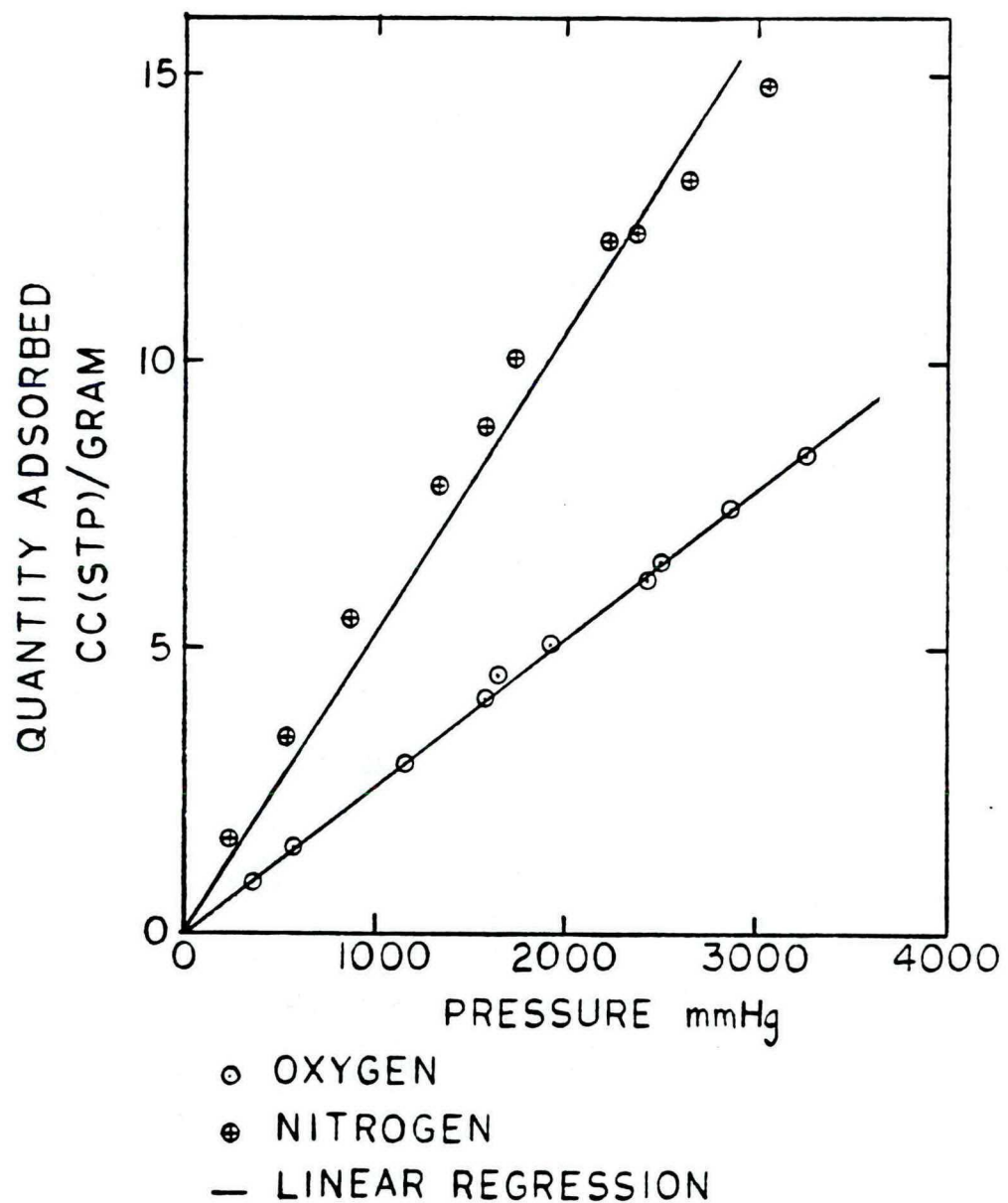


FIGURE 6: EQUILIBRIUM ISOTHERMS OF
 N_2 AND O_2 ON 5A AT $60^\circ C$

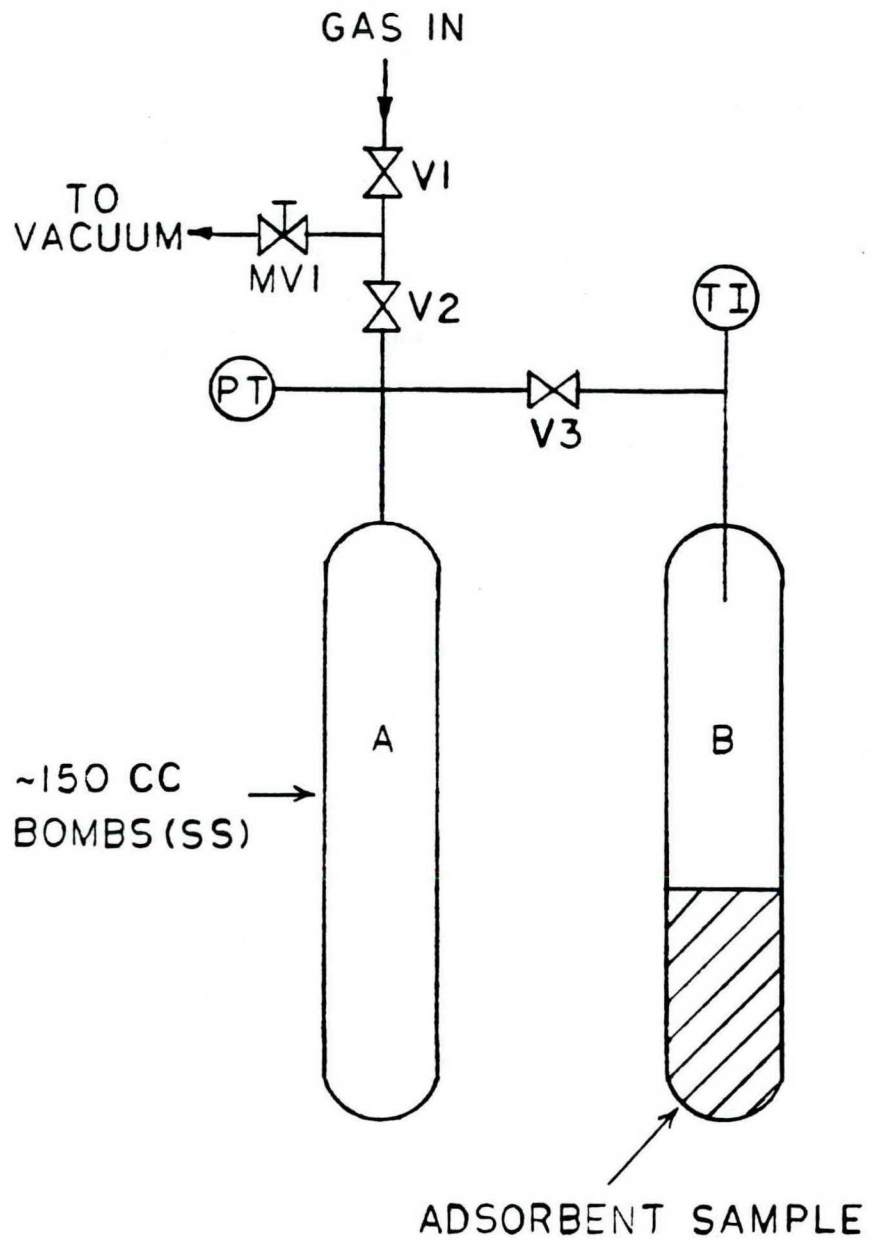


FIGURE 7: ADSORPTION EQUILIBRIUM APPARATUS

density determined in the previous section. Cautious use of isotherm data from the literature is suggested since standard definitions of the particle density and void fraction of zeolites have not been adopted.

As Figures 5 and 6 indicate, the nitrogen isotherms at 45°C and 60°C are approximately linear. Oxygen isotherms are linear for the entire range of temperatures and pressures studied. The constraint of linear, uncoupled isotherms should be reasonably supported for the nitrogen (A) - oxygen (B) binary up to 3500 mmHg at 45°C and 60°C.

Table 2: Linear Regression of Equilibrium Data

Gas	T °C	$\frac{k_i}{\text{cc (STP)}} \frac{\text{gm}}{\text{mmHg}}$	$\frac{K_i}{\text{gmoles/cc solid}}$ $\frac{\text{gmoles}}{\text{cc gas}}$
N ₂ (A)	30	0.00759	9.94
N ₂ (A)	45	0.00600	8.24
N ₂ (A)	60	0.00525	7.55
O ₂ (B)	30	0.00413	5.40
O ₂ (B)	45	0.00328	4.51
O ₂ (B)	60	0.00259	3.72 ₃

i = A or B

B. Experiments Designed to Test the Theory

1. Breakthrough Experiments

A breakthrough experiment consists of imposing a square wave change in feed gas composition and measuring the composition versus time profile of the effluent gas. As mentioned earlier, if the feed gas is enriched in species A and enters a bed dilute in A then in theory the effluent gas composition eventually undergoes a square wave or shock change. For the case when enriched B enters a bed dilute in B a simple-wave is generated. Both the shock-wave and simple-wave breakthrough experiments can be used to study the theory. The time that it takes the waves to exit the bed enables calculation of the slope of equilibrium isotherms. The shock-wave time, however, can be measured more precisely than the simple-wave time. Consequently, shock-wave breakthrough experiments are preferred and are studied here.

Equation [1] of the theory can be rearranged as follows (note that $t_{SH} = t_H$ and $U_H = U_{IN}$):

$$K_A = \left(\frac{U_{IN} t_{SH}}{L} - 1 \right) \left(\frac{\epsilon}{1 - \epsilon} \right) \quad [13]$$

K_A , the slope of the equilibrium isotherm of the preferentially adsorbed species, can be determined by measuring the terms on the right hand side of the equation above. To evaluate the isotherms of

nitrogen (A) by breakthrough experiments the light component used is oxygen (B). To evaluate the isotherms of oxygen (A) by breakthrough experiments the light component used is argon (B). Actually, oxygen and argon exhibit essentially identical isotherms and perhaps components other than argon are preferable for studying oxygen (A). For example, oxygen (A) - helium (B) may be better.

The apparatus shown in Figure 8 is used to perform breakthrough experiments. Additionally, since the high pressure feed step of the PSA cycle is identical to a breakthrough experiment,* the PSA system discussed in the next section is also used to determine equilibrium isotherms. The operation of the apparatus in Figure 8 involves the switching of the feed gas from B to A at time zero while measuring and recording in time the effluent composition. Two measurements of time are necessary to determine t_{SH} . The first is the time for the composition shock-wave to traverse the bed, associated fittings, and analytical equipment. The second measurement is the time for the composition shock to pass through only the fittings and analytical equipment. The second measurement accounts for the distance velocity lag or space time of the system not including the bed. The time for the shock to traverse the bed, t_{SH} , is equal to the first time minus the second time.

* This is true if the composition shock reaches the end of the bed exactly at the end of the feed cycle and under the conditions that the bed is initially purged and pressurized with pure light component.

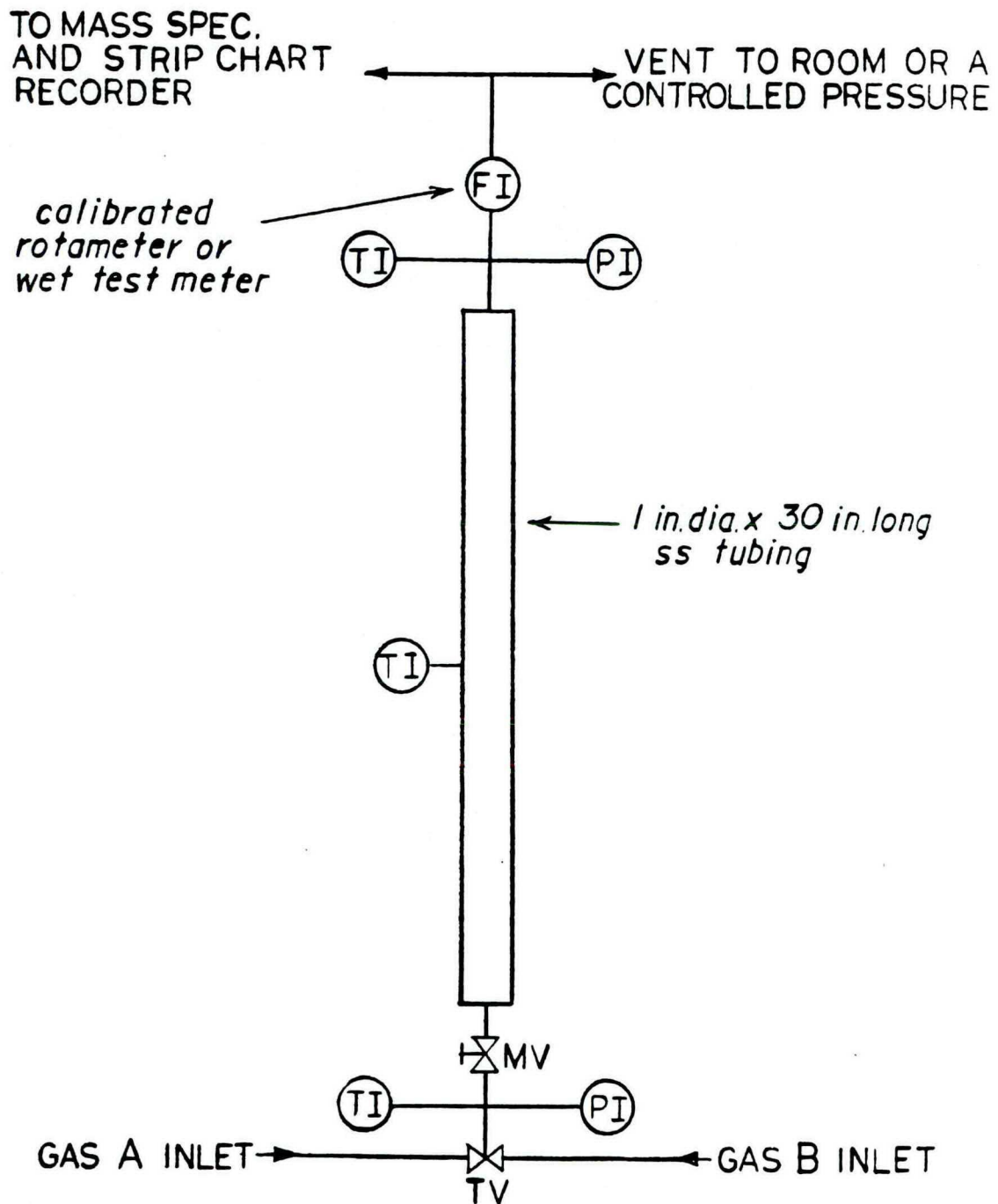


FIGURE 8: DIAGRAM OF BREAKTHROUGH UNIT

Table 3 represents the results of six breakthrough experiments. The agreement between the values obtained by breakthrough experiments and equilibrium experiments is quite good. The PSA method may be more reliable for performing breakthrough determinations of the slopes of equilibrium isotherms as Table 3 indicates.

Table 3: Equilibrium Isotherms From Breakthrough Experiments

Binary	Method*	P (psia)	T °C	U _{IN} cm/sec	K _{A, BR}	K _{A**} (equil)	Δ % rel. to K _A
N ₂ (A)-O ₂ (B)	1	3.315	24	14.20	23.66	23.62	+ 0.2
N ₂ (A)-O ₂ (B)	2	45.21	45	7.48	8.59	8.24	+ 4.2
N ₂ (A)-O ₂ (B)	2	43.85	60	6.40	7.22	7.55	- 4.4
O ₂ (A)-Ar(B)	1	14.51	20	3.88	7.21	6.94	+ 3.9
O ₂ (A)-Ar(B)	1	14.53	45	4.24	4.99	4.51	+10.6
O ₂ (A)-Ar(B)	1	14.56	60	4.44	4.05	3.72 ₃	+ 8.8

Average absolute Δ% = 5.4

* Method 1 - using apparatus of Figure 8, Method 2 - PSA system presented later.

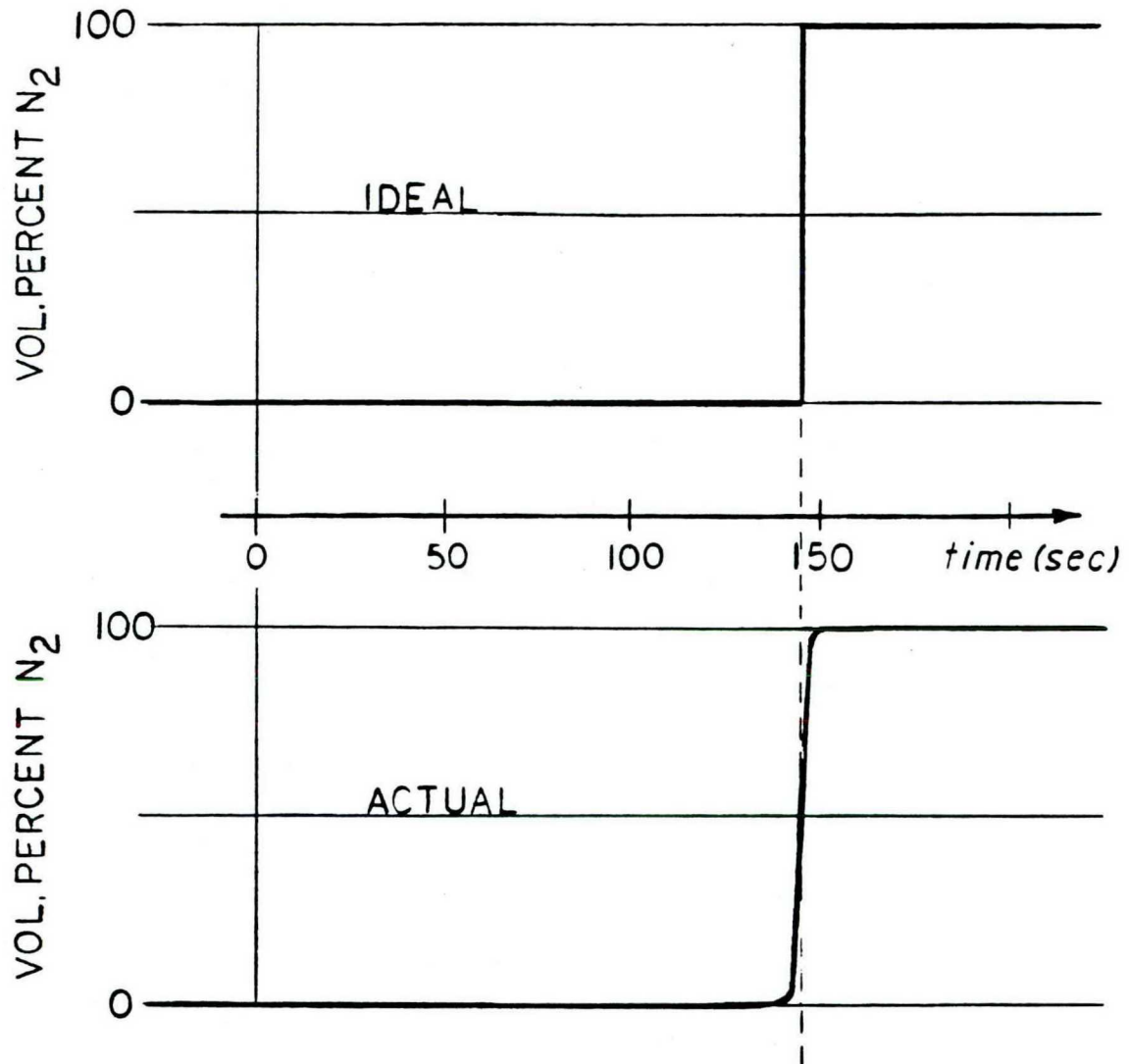
** 24°C nitrogen and 20°C oxygen equilibrium isotherms extracted from data of Miller [11].

The breakthrough experiments are performed at low feed rates resulting in small interstitial velocities. Reduced interstitial velocities support many of the assumptions of the theory as discussed below.

Local equilibrium - Local equilibrium is equivalent to assuming instantaneous adsorption and desorption rates. The assumption is a reasonable one for light gases on zeolites if the gas velocity is low enough through the packed bed to enable equilibrium to be approached.

Negligible axial dispersion - The dispersion coefficient, which is a measure of the dispersion forces in a flowing system, can be roughly separated into two components: one due to mixing at high velocities and one due to molecular diffusion. The use of low interstitial velocities diminishes the importance of the mixing component. The molecular diffusion component is not expected to be significant.

A good test of the local equilibrium and negligible axial dispersion assumptions is the shape of the breakthrough curves. A perfect composition shock-wave cannot exist since in real systems dissipation due to diffusion and dispersion occur. The prediction of a composition shock-wave is, nevertheless, an excellent approximation for the conditions studied as the typical breakthrough curve given by Figure 9 indicates. The experimental breakthrough



ACTUAL DATA FROM
 $N_2(A) - O_2(B)$ AT 3 PSIA
 (SEE TABLE 3).

*breakthrough
time*

FIGURE 9: ACTUAL & IDEAL BREAKTHROUGH CURVES

curves conclusively support the approximate validity of local equilibrium and negligible dispersion for the conditions studied.

Negligible axial pressure gradient - At low interstitial gas velocities the requirement of negligible pressure drop is approximated. To account for pressure drop in breakthrough calculations the inlet interstitial velocity is calculated at the average bed pressure at the point of breakthrough. At atmospheric pressures and greater, the pressure drop is small in comparison to the absolute pressure for the flow rates being studied.

Isothermal operation - The thermal effects of adsorption are mild but noticeable. During a nitrogen (A) - oxygen (B) breakthrough experiment the temperature in the beds of this study increase by as much as 5°C depending on the conditions of the experiment. At lower pressures and higher temperatures the quantity of material adsorbed decreased, resulting in a better approximation of isothermal operation. The inlet interstitial velocity used in breakthrough calculations is evaluated at the average bed temperature at the point of the composition shock breakthrough.

2. PSA Experiments

Figure 10 is a diagram of the process used to analyze PSA performance. The process is built to operate on the six-step cycle of Figure 1. The theoretical recovery (Eq. [9]) can be tested by

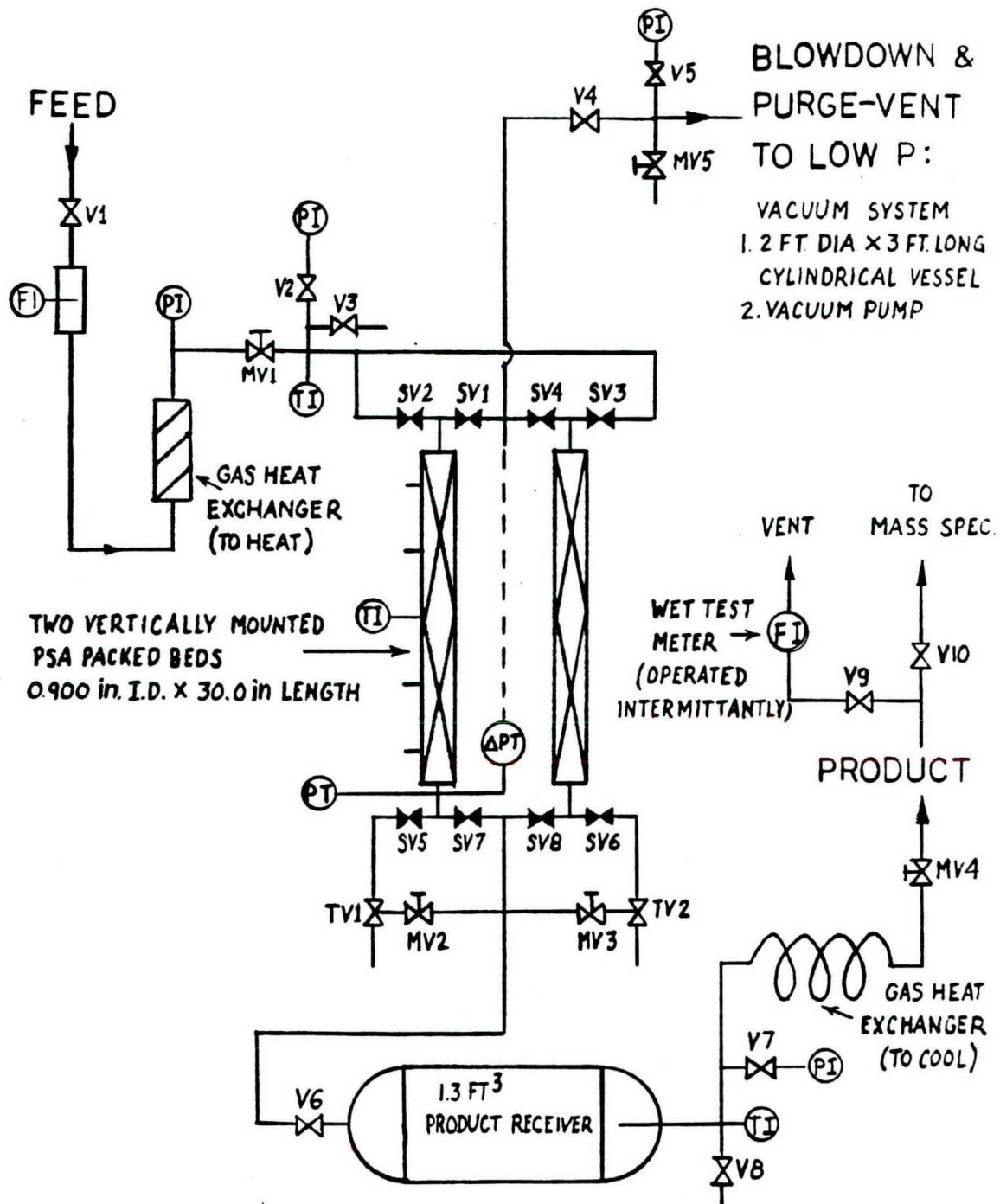


FIGURE 10: TWO-BED PSA PROCESS DIAGRAM

comparison with experimental recoveries measured using the system. The PSA process description and results are conveyed using the following format:

- a. Mechanical Operation
- b. Comments Concerning the Validity of the Theory
- c. Results
- d. Breakthrough Experiments Using the PSA System at 30°C - Nonlinear Nitrogen Isotherm
- e. Comments Concerning Experimental Error

a. Mechanical Operation

By comparing a theoretical, ideal six-step cycle to the actual six-step cycle the motivations for the scale of the process equipment, flow and pressure control strategy and other considerations are made clear. Figure 11 depicts the ideal pressure versus time functionality which the two-column, six-step process of Figure 1 experiences during a complete cycle. The theory requires the feed and purge steps to occur at constant pressure with negligible pressure drop. It is desired to mimic the ideal behavior of Figure 11 in the actual process.

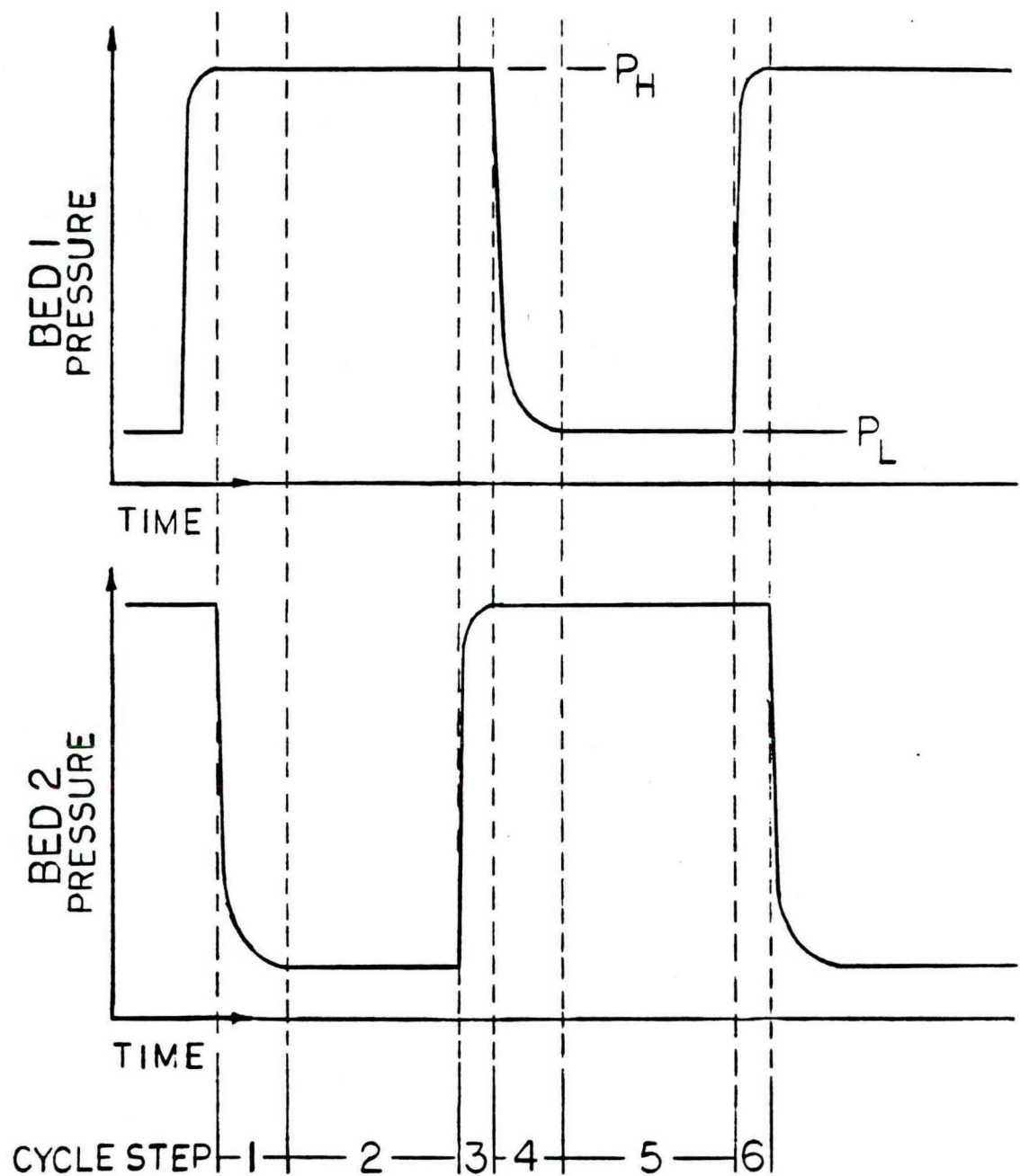


FIGURE 11: PRESSURE-VS-TIME FOR
AN IDEAL SIX-STEP CYCLE

Figure 12 is a typical pressure versus time plot experienced by the actual two-column process of Figure 10.* Table 4 lists the solenoid valves which are open for each cycle step. Using Table 4 and Figures 1 and 8 the detailed structure of Figure 10 is easily explained.

Table 4: Solenoid Valve Positions for Six-Step Cycle

Step	Valves Open
1	2, 4, 7
2	2, 4, 6, 7
3	2, 7, 8
4	1, 3, 8
5	1, 3, 5, 8
6	3, 7, 8

The profile of Figure 12 is due in part to the feed and product flow control strategy. The molar feed rate is maintained at a constant value by operating MV1 under critical flow conditions with constant upstream pressure and temperature. Critical flow ensures that pressure fluctuations downstream of MV1 do not affect the molar feed rate. The product flow through MV4 also occurs in the critical

* Pressure is measured using the pressure transducers and plotted by a stripchart recorder.

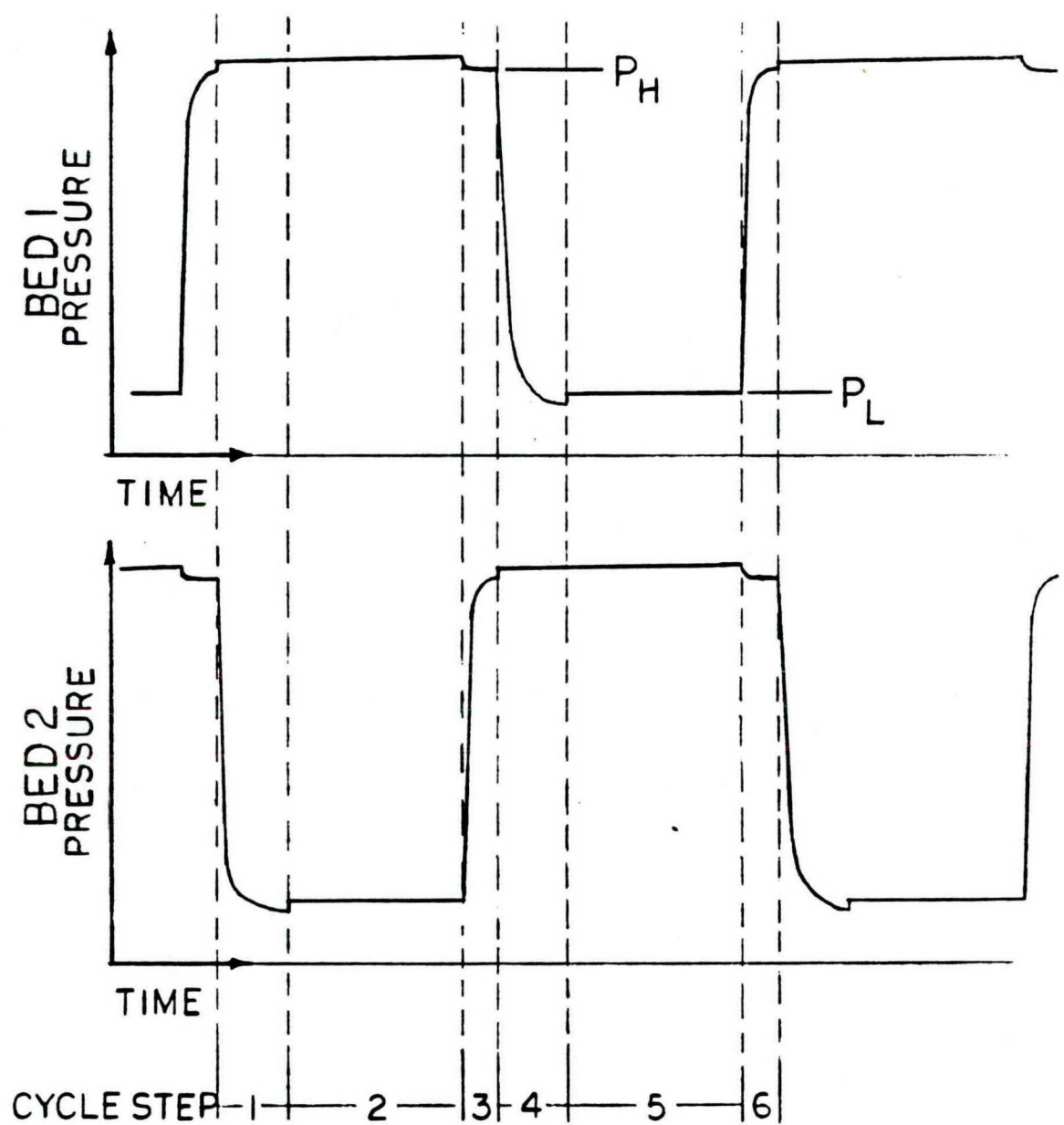


FIGURE 12: AVE. BED PRESSURE-VS-TIME FOR
AN ACTUAL SIX-STEP CYCLE

regime, but the flow rate is only approximately constant for reasons discussed below.

The pressure upstream of MV4 varies primarily because the pressurization with product step causes the pressure in the product receiver and column at high pressure to drop (see Figure 12). Consequently, the critical flow through MV4 varies since it is proportional to the upstream pressure. The percentage drop in the pressure caused by the pressurization step is less than 3% for all experiments because of the large volume product receiver. Since the pressure of the receiver drops during each pressurization step, it must increase during the other steps. The product valve, MV4, is set to allow pressure to increase properly after a pressurization step. The setting of MV4 thus ensures that the pressure is controlled from cycle to cycle. Furthermore, since the pressure fluctuations in the product receiver are small the product flow rate is only slightly variable. During product flow measurements a wet test meter is monitored over many process cycles to ensure that a mean value for the flow is obtained.

In Figure 12 it is evident that there is a pressure increase in a given bed when switching from the blowdown to purge steps. A similar increase also occurs when switching from the pressurization to high pressure feed steps. The increase is attributable to the pressure drop induced by the purge and feed flows. Only for low pressure purge steps occurring below 5 psia does the total pressure drop exceed 10% of the inlet pressure. For the high pressure feed

step, the total bed pressure drop is only about 1% of the inlet pressure for the conditions studied. The assumption of negligible pressure drop used in the theory is not always true but calculations can be performed using the average bed pressure with little loss in accuracy.

There are several facets to the design of the PSA process which are not apparent in Figure 10. For example, the open volume of the fittings between the solenoid valves and packed columns is minimized relative to the volume of the beds to avoid the loss of product which may fill the voids and be lost during the blowdown and purge steps. To minimize the void space the solenoid valves are connected directly to the beds using the minimum of fittings. In addition, 30" long beds are employed making the total void space only about 2% of the volume of the columns. The solenoid valves are thus essentially at the ends of the packed beds which is implicitly required by the theory. Additional detailed design information is given in the Appendix.

In conclusion, the process in Figure 10 can be expected to mechanically behave as the ideal cycle of Figure 11. A comparison of the ideal and actual process pressure versus time behavior is made for a single column in Figure 13. The approximation is good primarily because of the large product receiver. The large receiver, however, causes the product composition to respond very slowly to process changes (e.g. feed flow rate). It is therefore

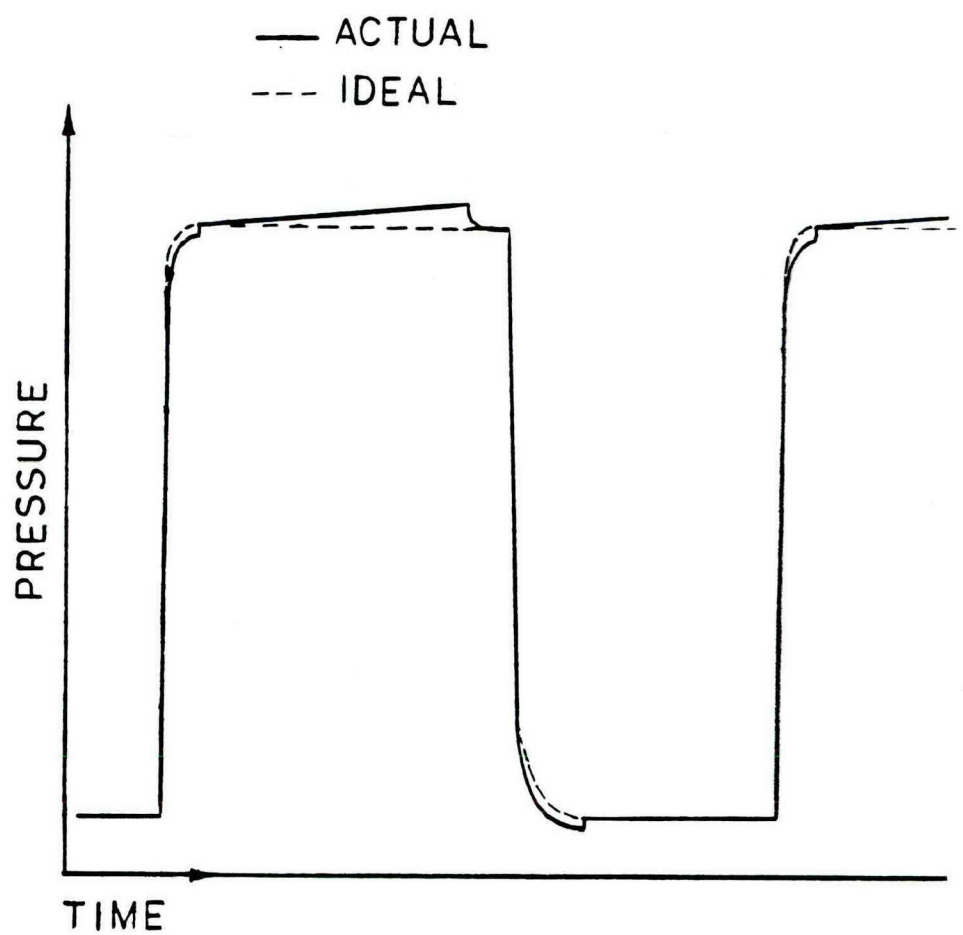


FIGURE 13: IDEAL-VS-ACTUAL PRESSURE SWING CYCLES

necessary to operate the process patiently to ensure that steady state is attained.

b. Comments Concerning the Validity of the Theory

It is noted above that the actual PSA cycle approximates the pressure cycling of an ideal process. Several other approximations are discussed here. The comments in the breakthrough section pertaining to low interstitial velocities are applicable to the operation of the PSA process. Interstitial velocities of less than 10 cm/sec are used in the experimental study for both feed and purge steps. In fact, as Table 3 indicates, Equation [1] of the theory is quite accurate for the interstitial velocities of the high pressure feed step of the PSA cycle studied here.

Binary Mixture - The air used in PSA experiments contains three components: nitrogen ($\sim 78\%_{vol.}$), oxygen ($\sim 21\%_{vol.}$), and argon ($\sim 1\%_{vol.}$). Argon adsorption on molecular sieve 5A from $0^{\circ}C$ to $100^{\circ}C$ and up to 4000 mmHg is essentially identical to that of oxygen (i.e. the adsorption isotherms are coincident). The oxygen-argon pair is therefore treated as a single component and the mixture as a binary.*

* The following relation holds $\left. \frac{\%Ar}{\%O_2} \right|_{FEED} = \left. \frac{\%Ar}{\%O_2} \right|_{PRODUCT} = 0.045$

given the feed gas composition of $0.94\%_{vol.}$ Ar, $20.9\%_{vol.}$ O_2 , and $78.16\%_{vol.}$ H_2 .

Identical Columns - The two columns of the PSA system are of identical length and diameter. The void fractions of bed 1 and bed 2 are essentially equal at 0.479 and 0.481, respectively. A value of 0.480 is used in all calculations.

Isothermal Operations - The maximum temperature variation observed during a typical PSA cycle (e.g. $P_H = 45$ psia, $P_L = 5$ psia, $T = 45^{\circ}\text{C}$) is $\pm 4^{\circ}\text{C}$. The adsorption during the high pressure feed step generates the high temperature during the cycle while the blowdown and purge generate the low temperature. The temperature variations affect the quantity adsorbed and to a lesser extent the gas density. The net total effect of temperature variations over an entire cycle is difficult to predict. The results of the recovery experiments indicate that $\pm 4^{\circ}\text{C}$ is close enough to isothermal operation to neglect thermal effects.

C. PSA Results

The theory postulates complete clean up of the light component and recovery of the light component given by Equation [9] restated here.

$$R_{TH} = (1 - \beta) \left(1 - \frac{1}{\rho(1 - \gamma_F)} \right) \quad [9]$$

The experimental results to compare with theory are the product purity and the recovery. The recovery of the light component for

the PSA process of Figure 10 is simply the ratio of the product rate of light component divided by the feed rate of light component. The variables studied are β and P while Y_F is constant in all experiments. β is calculated using the equilibrium adsorption isotherm slopes presented in Table 2. β is weakly temperature dependent equaling 0.593 at 45°C and 0.548 at 60°C. The pressure ratio, P , is varied by adjusting the blowdown pressure and the purge flow rate. The blowdown pressure can be varied by controlling the pressure of the 3' long x 2' diameter low pressure vessel attached to a vacuum pump system. The purge flow rate is adjusted by setting MV2 and MV3 equally at a specific flow rate. Table 5 summarizes the results. Figure 14 is a plot of the 45°C data of Table 5. The data clearly indicate the experiments are well approximated by the theory for both product purity and product recovery.

Table 6 is a typical cycle time breakdown used in the PSA studies. Cycle times for each experiment, procedures, calculations, and statistical information for each experiment are summarized in the Appendix.

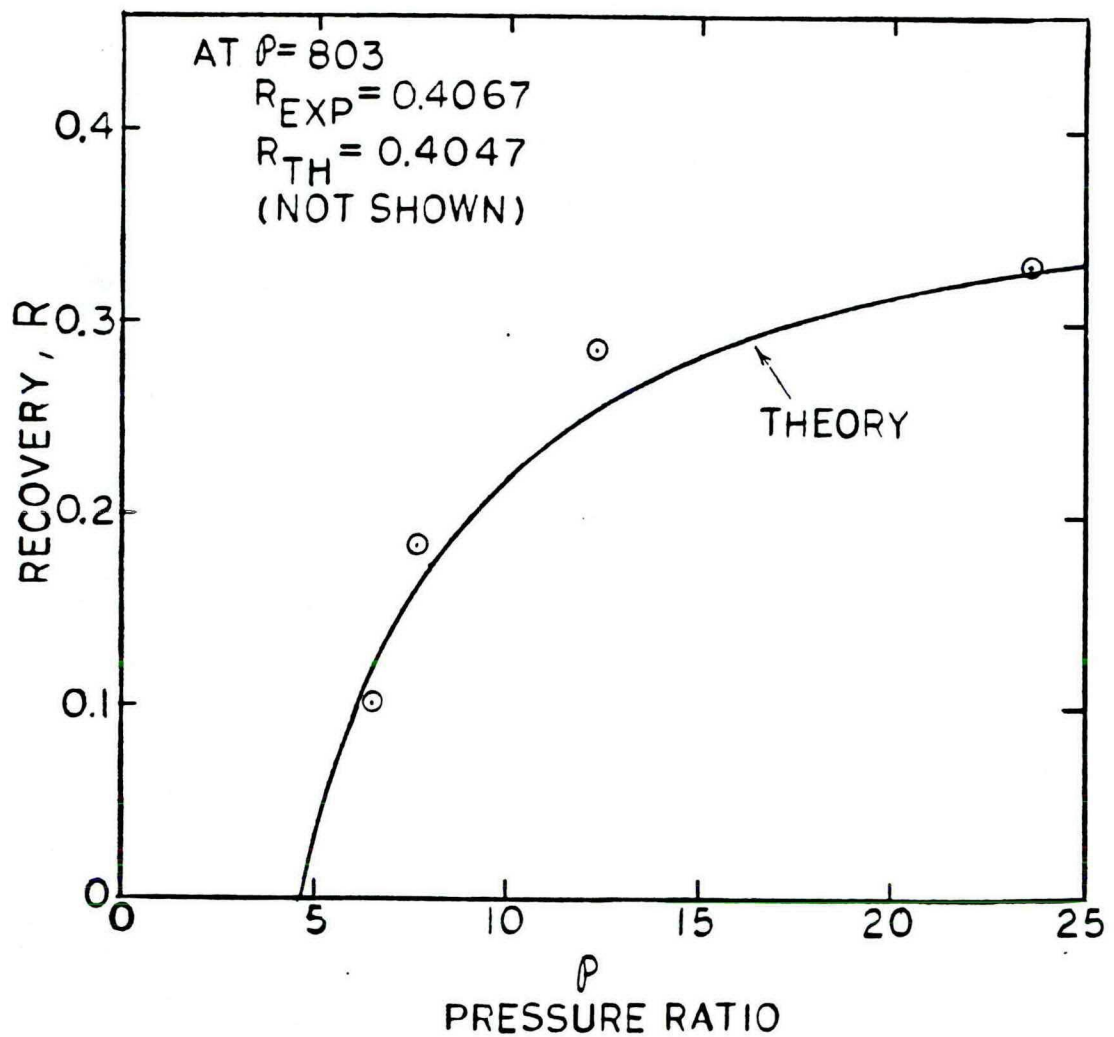


FIGURE 14: OXYGEN RECOVERY AT 45°C

Table 5: PSA Recovery Data, O₂ + Ar From Air

Run*	P _H psia	**	o _C T % vols.	(O ₂ +Ar) PROD. SLPM	Q _{IN} SLPM	R _{EXP}	R _{TH}	Δ % rel. to EXP
1	44.75	6.476	45	99.72	2.342	0.1017 ₄	0.1179	+15.9
2	45.46	7.695	45	99.74	2.342	0.1838	0.1637	-10.9
3	45.30	12.36	45	99.75	2.333	0.2870	0.2556	-10.9
4	43.95	23.54	45	99.80	2.314	0.3294	0.3275	-0.6
5	45.60	803	45	99.27	2.344	0.4067	0.4047	-0.5
6	43.85	840	60	99.34	1.851	0.4332	0.4492	+3.7

Ave. absolute Δ% = 7.1

* Each run represents the average of 2-6 hours of data collection at steady state.

** For runs 5 and 6 the large pressure ratio is obtained by operating at a blowdown pressure of <3 mmHg. The purge step is not necessary for runs 5 and 6 since N_H = P.

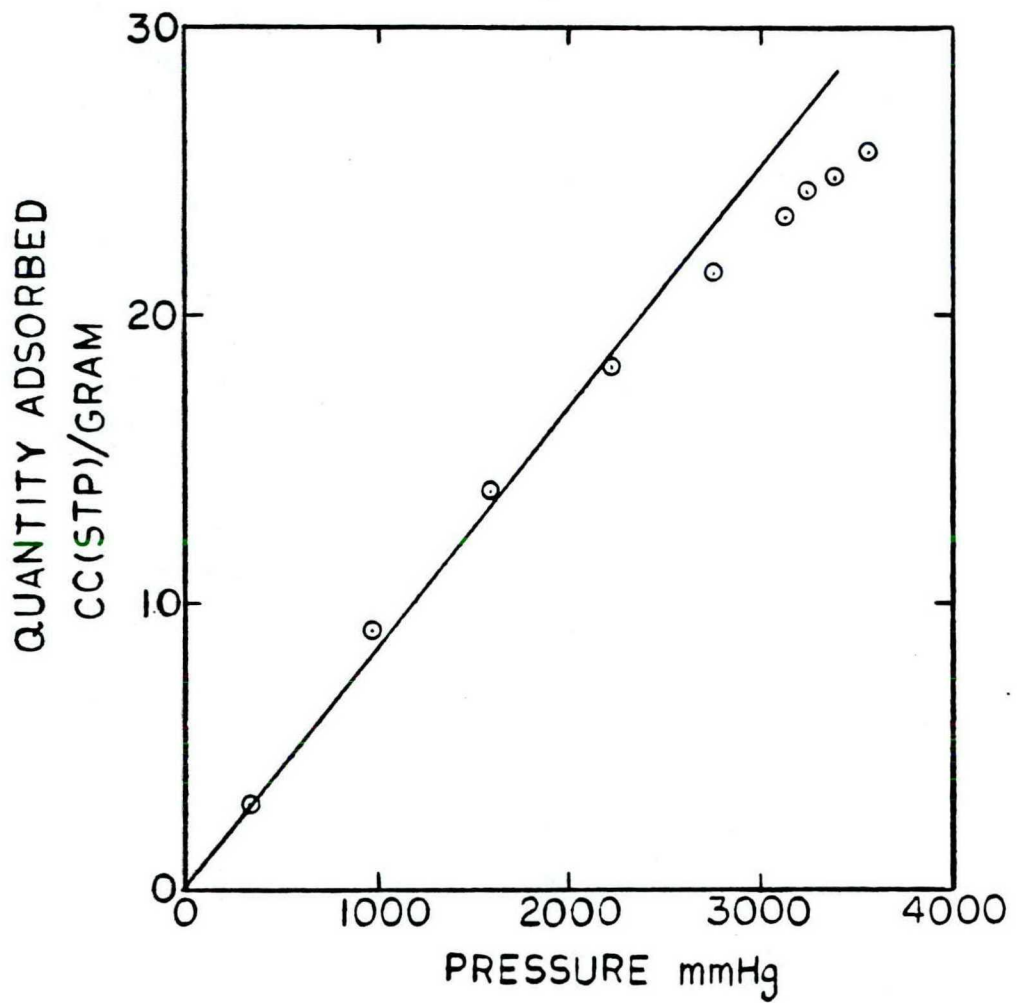
—
N_L

Table 6: Typical Cycle Times (Runs 1-4)

Step	Time (Sec)	
1	35	
2	65	$t_H = t_{SH}$
3	5	
4	35	
5	65	
6	5	
210 sec		

D. Breakthrough Experiments at 30⁰C Using PSA System

The results of a single breakthrough experiment performed at 30⁰C are presented in Table 7. Since the isotherm of nitrogen at 30⁰C is notably nonlinear, the breakthrough experiment determines an effective linear isotherm using Equation [1]. Figure 15 is a plot of the effective isotherm and the actual isotherm. The intersection of the curves occurs at 2075 mmHg.



⊕ NITROGEN EQUILIBRIUM DATA

- $K_{BR_{eff}}$

FIGURE 15: NITROGEN BREAKTHROUGH AT 30°C

Table 7: Nitrogen Breakthrough at 30°C*

P psia	T °C	U_{IN} cm/s	$\frac{L}{tSH}$ cm/s	$K_{A,BR}_{eff}$	$k_{A,BR}_{eff}$ cc(STP) gm mmHg
45.89	30	7.521	0.5862	10.92	0.00834

* Data represents the average of four data points.

It may be possible to measure nonlinear isotherms via breakthrough experiments. The partial pressure of nitrogen in the experiment is 1860 mmHg. A value of $K_{A,eff}$ calculated from the slope of a line passing through the origin and the actual isotherm at 1860 mmHg is only 3.1% higher than $K_{A,BR}_{eff}$ of Table 7. The measurement of $K_{A,BR}_{eff}$ at several feed partial pressures of the strongly adsorbed component may allow the nonlinear isotherm to be constructed. That is, a point on the actual equilibrium isotherm may be given by the value of the linear effective isotherm with slope $K_{A,BR}_{eff}$ at the feed partial pressure of A used to measure $K_{A,BR}_{eff}$.

e. Comments Concerning Experimental Error

Definitive statements concerning the reasons for the differences between experimental and theoretical values of the

recovery are difficult to make. The error in the recovery data is attributable to many factors, several of which cannot, at present, be quantified. While every attempt is made to run experiments under conditions where the theory is valid, the mild thermal effects, imperfect mechanical design, effects of nonzero pressure drop during feed and purge steps, and the inability to operate the process exactly at the limit* are all effects which generate errors which are difficult to evaluate. A larger data bank including replicative measurements is needed. It is clear, however, that the errors (both random and systematic) are not large, as Table 5 indicates.

The data indicate that the error increases as the pressure ratio decreases. This is primarily because the product flow rate decreases as the pressure ratio decreases. For example, in Run 3 the experimental product flow rate is 146 cc(stp)/min and the theoretical value based on the feed rate is 130 cc(stp)/min. The $\Delta\%$ error is -10.9 and the difference in flow is 16 cc(stp)/min. In Run 1 the $\Delta\%$ error is +15.9 while the difference in product flow between experiment and theory is only 8 cc(stp)/min. Accounting for 16 and 8 cc(stp)/min out of \sim 2300 cc(stp)/min entering as feed could be attributed to any of several different factors. Singling

* For the process to be operated at the limit, the composition shock-wave occurring during the high pressure feed step must reach the end of the bed exactly and the purge flow must be the minimum required to complete the heavy component removal during the purge step.

out the dominant causes of error is not a simple task and is not possible with the amount of data collected to date.

CHAPTER IV

CONCLUSIONS AND RECOMMENDATIONS

The experimental data indicate the PSA model of Knaebel and Hill [8] is accurate for the experimental conditions tested. Application of the theory to breakthrough experiments enables prediction of the slope of linear equilibrium isotherms with an average absolute error of 5.4% relative to actual equilibrium values. In PSA experiments the theory predicts recovery of the light component with an average absolute error of 7.1% relative to experimental values. The theory claims complete clean-up of the light component while product purity in the laboratory is never less than 99.2%_{vol.} and averages 99.6%_{vol.} in the light component. The differences between the theory and the experiments is attributable to experimental error, minor violations of the assumptions and constraints of the theory (i.e., $\Delta P \neq 0$, $T \neq$ constant), and imperfect mechanical design.

The equations of the theory are directly applicable to the entire design of a PSA process when the assumptions and constraints are approximated. The necessary physical property input data to the theory are the void fraction and the slopes of the adsorption isotherms. The void fraction can be measured using the technique

described in Chapter III. The accuracy of the void fraction determined using the technique is evidenced by its use in the successful application of the theory to the breakthrough and PSA process experiments. The slopes of the linear equilibrium adsorption isotherms can be obtained by running simple breakthrough experiments.

The experimental data collected thus far are almost entirely for conditions which do not significantly violate the assumptions and constraints of the model of Knaebel and Hill [8]. Consequently, there is considerable need for theoretical analysis coupled with experimental work to further develop the understanding of PSA processes. The assumptions and constraints of the model [8] are an excellent framework for further study. The effect of nonlinear isotherms (briefly examined in breakthrough experiments in this work), faster cycling (i.e. increased throughputs), and the effects of temperature variations are good places to start. It is anticipated that when the assumptions and constraints are relaxed, the parameters of the model [8] (e.g. β_i , P), perhaps in a modified form, will still be important.

NOMENCLATURE

Equations and Tables

A_{CS}	cross sectional area, cm^2
β	a separation factor defined by equation [10], —
β_i	component i term defined by equation [3], —
ϵ	void fraction, —
E_B	effluent product rate of component B, $1/\text{min}$
F_B	feed rate of component B, $1/\text{min}$
K_i	slope of the equilibrium isotherm of component i, $\frac{\text{gm moles/cc solid}}{\text{gm moles/cc gas}}$
$K_{A,BR}$	slope of the equilibrium isotherm of A from breakthrough experiments, $\frac{\text{gm moles/cc solid}}{\text{gm moles/cc gas}}$
$K_{A,BR}_{\text{eff}}$	effective slope of a nonlinear isotherm from breakthrough experiments, $\frac{\text{gm moles/cc solid}}{\text{gm moles/cc gas}}$
$K_{A,\text{eff}}$	effective slope of a nonlinear isotherm predicted on the basis of partial pressure of A, $\frac{\text{gm moles/cc solid}}{\text{gm moles/cc gas}}$
k_i	slope of the equilibrium isotherm of component i, $\frac{\text{cc(STP)}}{\text{gm mmHg}}$
L	length of a column, cm

N_H	moles feed at high pressure for the high pressure feed step, gm moles
N_{HP}	moles of product exiting a bed for the high pressure feed step, gm moles
N_L	moles of purge gas added for the low pressure purge step, gm moles
N_{PR}	moles of gas to pressurize a bed, gm moles
P_H	average bed pressure during high pressure feed, psia
P_L	average bed pressure during low pressure purge, psia
ρ	pressure ratio defined by equation [11], —
ΔP_H	pressure drop during high pressure feed step, psi
ΔP_L	pressure drop during low pressure purge step, psi
Q_{IN}	volumetric flow rate of feed, l/min at a given T and P
R	recovery, $\frac{\text{Product B}}{\text{Feed B}}$
R_{EXP}	experimental recovery
R_{TH}	theoretical recovery
R_g	universal gas constant, 82.05 $\frac{\text{cc atm}}{\text{gm mole } ^\circ\text{K}}$
ρ_B	bulk density, gm/cc
ρ_L	liquid density, gm/cc
ρ_P	particle density, gm/cc
t_H	time for the high pressure feed step, sec
t_L	time for the low pressure purge, sec
t_{SH}	time for the composition shock to traverse a bed, sec
T	temperature, $^\circ\text{K}$

U_{IN}	interstitial velocity of the feed gas to a column, cm/sec
U_L	interstitial velocity of the low pressure purge gas at inlet, cm/sec
U_H	interstitial velocity of high pressure fed gas at inlet, cm/sec
U_{SH}	velocity of composition shock-wave, cm/sec
V	volume, cm^3
w_i	weight of object i , gms
γ_E	mole fraction of A in the effluent product gas, —
γ_F	mole fraction of A in the feed gas, —
Z	axis of the column or packed bed, cm

Figures

V	valve
MV	metering valve (0.020 in. orifice)
TV	two-way valve
SV	solenoid valve
PI	pressure indicating gauge
PT	pressure transducer
ΔPT	delta pressure transducer
TI	temperature indicator
FI	flow indicator

REFERENCES

1. Davis, J. C., Chem. Engineering, 79 (10) 88, (1972).
2. Lee H., and D. E. Stahl, AICHE Symp. Ser., 69 (134) 1, (1973).
3. Keller, G. E., and R. L. Jones, ACS Symp. Series, No. B5, 275 (1980).
4. Alexis, R. W., Chem. Eng. Prog., 63, 69 (1967).
5. Cassidy, R. T., ACS Symp. Series, No. 135 (1980).
6. Skarstrom, C. W., Ann. N.Y. Acad. Sci., 72, 751 (1959).
7. Skarstrom, C. W., Recent Developments in Separation Sciences, Vol. 2, pp. 95-106. CRC Press, Cleveland, OH. (1972).
8. Knaebel, K. S. and F. B. Hill, Chem. Eng. Sci., (submitted 1982).
9. Chan, Y.N.I., F. B. Hill, and Y. W. Wong, Chem. Eng. Sci., 36, 243 (1981).
10. Shendelman, L. H., and J. E. Mitchell, Chem. Eng. Sci., 27, 1449 (1972).
11. Miller, G. W., Master's Thesis, Ohio State Univ., (1984).

APPENDIX

PROCEDURES, DATA, CALCULATIONS

- A. Activation of Zeolite
- B. Void Fraction Determination
- C. Equilibrium Isotherm Measurement
- D. Breakthrough Experiments
- E. PSA Process Experiments
- F. Equipment Summary

A. Activation of Zeolite

Regeneration of zeolite is performed by heating the sample to 350°C at less than 0.1 mmHg pressure for eight hours. At these conditions the zeolite is essentially stripped of the strongly adsorbed species--especially water. Eight hours is used in this study as a regeneration time since longer times do not affect the zeolite weight, indicating that the regeneration is complete.

B. Void Fraction Determination

a. Procedure (Refer to Figure 3)

1. Weigh glass, W_g .
2. Fill AA' with liquid and weigh; determine volume of AA' section, $V_{AA'}$
3. Fill BB' with liquid and weigh; determine volume of BB' section, $V_{BB'}$
4. Fill AB (entire volume) with solvent and weigh; determine volume of A'B' section, $V_{A'B'}$

Comment: Repeat steps 1-4 five times.

5. Pack glass column between A' and B' with adsorbent and weigh; determine weight of solids, W_S .
6. Fill entire system with liquid and weigh, W_T ; determine porosity using the following equation:

$$W_T = W_g + V_{AA'} \rho_L + V_{BB'} \rho_L + W_S + \epsilon V_{A'B'} \rho_L$$

Comment: Repeat steps 5 and 6 five times. The liquid should be degassed to minimize bubble formation in the packed bed during filling. The liquid should be admitted slowly to the apparatus.

b. Data and Calculations

1. $W_g = 187.40 \pm 0.00$ gms, $n = 5$
2. $W_{AA'} = 0.80 \pm 0.00$ gms, $n = 4$
3. $W_{BB'} = 10.63 \pm 0.05$ gms, $n = 4$
4. $W_{AB} = 119.78 \pm 0.05$ gms, $n = 4$

Comment: Liquid used is C_6H_{12} . $\rho_L = .779^{20/4}$. Experimental temperature is $20^{\circ}C$.

$$V_{AA'} = 1.03 \text{ cc} \quad V_{BB'} = 13.65 \text{ cc} \quad V_{AB} = 153.76 \text{ cc}$$

$$V_{A'B'} = 130.08 \text{ cc}$$

$$5. \text{ Run 1} \quad \epsilon = 0.492$$

$$\text{Run 2} \quad \epsilon = 0.477$$

$$\text{Run 3} \quad \epsilon = 0.463$$

$$\text{Run 4} \quad \epsilon = 0.476$$

————— with C_6H_{12} $\epsilon = 0.477 \pm 0.012$

$$\text{Run 5} \quad \epsilon = 0.481$$

————— with $n-C_{18}H_{38}$

$$\bar{\epsilon} = 0.478 \pm 0.010$$

6. Average bulk density of above runs is $\bar{\rho}_B = 0.810 \pm 0.002$
gm/cc

So, $\bar{\rho}_P = 1.552 \pm 0.030$ gm/cc (activated sieve 5A)

C. Equilibrium Isotherm Measurement

a. Procedure (Refer to Figure 7)

1. Activate zeolite.
2. Add known weight of activated zeolite to bomb B.
3. Pull a vacuum on entire equilibrium unit ($\ll 1$ mmHg).
4. Submerge apparatus in an isothermal bath at desired temperature.
5. Close V3. Add gas to bomb A and close V2. Monitor pressure until steady (i.e. until temperature equilibrates with bath). Record pressure.
6. Open V3. Wait for pressure to stabilize. Record pressure and temperature.

Comment: Assuming the volumes of A and B are known a mass balance allows the adsorption to be quantified. Assuming ideal gases the following equation is written:

$$\frac{P_A V_A}{RgT} \Big|_{t=0} = \frac{P_A V_A}{RgT} \Big|_{eq} + \frac{P_B \left[V_B - \bar{\rho}_P \right]}{RgT} \Big|_{eq} + n_{AD}$$

7. After a data point, V3 can be closed and additional gas can be added to or subtracted from bomb A. The moles added or subtracted can be calculated and V3 opened. The entire isotherm can be obtained by successively adding or subtracting gas from bomb A. Gas adsorption on zeolite is known to not exhibit hysteresis.

b. Data and Calculations

1. Determination of Volumes

Comment: A standard volume is calibrated by water displacement. The volume is then used to determine volumes A and B by gas displacement.

$$V \text{ (standard)} = 323.4 \pm 0.5 \text{ cc}, n = 4$$

Since two equilibrium systems are used, four volumes are determined.

System 1	System 2
$V_A = 163.36 \pm .2 \text{ cc}, n = 3$	$V_A = 164.17 \pm .24 \text{ cc}, n = 3$
$V_B = 161.66 \pm .27 \text{ cc } n = 3$	$V_B = 156.39 \pm .54 \text{ cc, } n = 3$

2. Weight of Zeolite

System 1	System 2
46.348 gms	43.383 gms

3. Tabulated Data and Calculations

Nitrogen on 5A

$P(\text{mmHg})$	30°C $\text{cc(STP)}/\text{gm}$	$P(\text{mmHg})$	45°C $\text{cc(STP)}/\text{gm}$	$P(\text{mmHg})$	60°C $\text{cc(STP)}/\text{gm}$
330	2.992	260	1.639	234.5	1.665
983	9.07	746	4.883	519.5	3.451
1597	13.94	1165	7.668	881.1	5.522
2222	18.23	1643	10.56	1320	7.87
2763	21.41	2168	13.48	1725	10.06
3122	23.37	2545	15.44	2223	12.10
3380	24.73	2972	17.52	2646	13.23
3555	25.66	3307	18.97	3055	14.82
3229	24.40	2662	16.37	2386	12.21
				1577	8.902

30°C Data: 1. Using Equilibrium system 2.

2. Plotted in Figure 4.

3. Linear regression: $k_A = 0.00759 \frac{\text{cc(STP)}}{\text{gm mmHg}}$

or $K_A = 9.94 \frac{\text{gm moles/cc solid}}{\text{gm moles/cc gas}}$

45°C Data: 1. Using Equilibrium system 2.

2. Plotted in Figure 5.

3. Linear regression: $k_A = 0.0060 \frac{\text{cc(STP)}}{\text{gm mmHg}}$

or $K_A = 8.24 \frac{\text{gm moles/cc solid}}{\text{gm moles/cc gas}}$

- 60⁰C Data:
1. Using Equilibrium system 1.
 2. Plotted in Figure 6.
 3. Linear regression: $k_A = 0.005249 \frac{cc(STP)}{gm\ mmHg}$
or $K_A = 7.55 \frac{gm\ moles/cc\ solid}{gm\ moles/cc\ gas}$

Comment: The linear regression used forces the fit through the origin.

$$y = bx$$

$$b = \frac{\sum(x_i y_i)}{\sum(x_i)^2}$$

Oxygen on 5A

<u>30⁰C</u>		<u>45⁰C</u>		<u>60⁰C</u>	
P(mmHg)	cc(STP)/gm	P(mmHg)	cc(STP)/gm	P(mmHg)	cc(STP)/gm
461.2	2.002	321.2	1.104	365	0.929
1262	5.510	784	2.698	578.7	1.500
1869	7.918	1328	4.508	1154	2.979
2378	9.948	1954	6.505	1585	4.077
2903	11.97	2429	7.98	1923	5.027
3249	13.26	2709	8.85	2440	6.202
3494	14.13	3012	9.78	2879	7.417
3626	14.65	3342	10.74	3272	8.352
3264	13.40	2619	8.64	2502	6.529
2782	11.69	1663	5.77	1643	4.592
2110	9.22				

30°C Data: 1. Using Equilibrium system 1.

2. Plotted in Figure 4.

3. Linear regression: $k_B = 0.00413 \frac{\text{cc(STP)}}{\text{gm mmHg}}$

$$\text{or } K_B = 5.40 \frac{\text{gm moles/cc solid}}{\text{gm moles/cc gas}}$$

45°C Data: 1. Using Equilibrium system 1.

2. Plotted in Figure 5.

3. Linear regression: $k_B = 0.00328 \frac{\text{cc(STP)}}{\text{gm mmHg}}$

$$\text{or } K_A = 4.51 \frac{\text{gm moles/cc solid}}{\text{gm moles/cc gas}}$$

60°C Data: 1. Using Equilibrium system 2.

2. Plotted in Figure 6.

3. Linear regression: $k_B = 0.00259 \frac{\text{cc(STP)}}{\text{gm mmHg}}$

$$\text{or } K_A = 3.723 \frac{\text{gm moles/cc solid}}{\text{gm moles/cc gas}}$$

Additional Equilibrium Data

Comment: The equilibrium data of Miller [11] is used for comparative purposes in the breakthrough experiments. The data is adjusted to the definition of particle density determined in this study. The following two linear isotherm values are used.

N_2 at 24°C and <3 psia : $K_A = 23.62 \frac{\text{gmoles/cc solid}}{\text{gmoles/cc gas}}$

O_2 at 20°C up to 14.696 psia : $K_B = 6.94 \frac{\text{gmoles/cc solid}}{\text{gmoles/cc gas}}$

D. Breakthrough Experiments

a. Procedure (Refer to Figure 8)

1. Regulate the pressure of the gases so that each gas is at the same pressure at the inlet. A pressure greater than twice the bed pressure is desired to create a critical flow situation at the metering valve (MV).
2. Adjust the metering valve (MV) so that a desired flow of gas A is obtained.
3. Let gas B purge the bed entirely.
4. "Instantaneously" turn the two-way valve to allow gas A to flow into the bed. Log the composition-vs-time curve.
5. Repeat steps 3 and 4 several times.
6. It is necessary to subtract out the dead time of the system by removing the packed bed and repeating steps 3 through 5 above.

b. Data and Calculations

Comment: The inlet gas velocity used in breakthrough experiments is calculated at the average pressure and temperature of the bed at the point of breakthrough.

EXPERIMENT

	1	2	3	4	5**	6
Binary*	O ₂ (A)-Ar(B)	O ₂ (A)-Ar(B)	O ₂ (A)-Ar(B)	N ₂ (A)-O ₂ (B)	N ₂ (A)-O ₂ (B)	N ₂ (A)-O ₂ (B)
\bar{T} (°C)	20	45	60	24	45	60
\bar{P} (psia)	14.51	14.53	14.56	3.315	45.21	43.85
$\Delta \bar{P}$ (psia)	0.135	0.174	0.232	0.63	0.632	0.645
\bar{t}_{SH} (sec)	174.25	117.0	93.85	145.1	105	105
\bar{U}_{IN} (cm/sec)	3.880	4.243	4.443	14.202	7.480	6.402
ϵ	0.478	0.475	0.475	0.476	0.480	0.480
A _{CS} (cm ²)	3.871	3.871	3.871	3.871	4.104	4.104
L (cm)	76.20	76.20	76.20	76.20	76.20	76.20
n # of runs	3	3	3	2	5	4
K _{A,BR}	7.21	4.99	4.05	23.66	8.59	7.22

* An overbar indicates the value is the average over n trials. For pressure and temperature the value is the average for the bed.

** Runs 5 and 6 represent average data from PSA operation.

Comment: K_{A,BR} is given by equation [13].

E. PSA Process Experiments

- a. Design Comments (refer to Figure 10)
1. The inlet gas heat exchanger consists of a 1 in. dia x 10 in. long tube packed with copper coated steel balls. A heating block is clamped on the outside of the tube and powered through a variac powerstat. By adjusting the variac the feed gas temperature downstream of MV1 is controlled.
 2. The packed columns are fit into an aluminum metal block to allow for symmetric and thus equal wrapping of the beds with electrical heating tape. The symmetric heating enables the temperature monitoring to be limited to just one bed. The power to the heating tape is supplied through a variac powerstat.
 3. The product receiver is covered by a silicone heating blanket which is powered through a variac powerstat.
 4. The packed columns, associated fittings, and the product receiver are all insulated either with 1/2" thick foam insulation or pipe duct formed fiberglass insulation.
 5. The packed beds are supported internally by gas distribution plates. The plates are thin brass discs drilled with approximately 40 holes of 0.020 in. diameter.

6. As noted in the text of this report, the solenoid valves are as close to the packed columns as possible to minimize void spaces.
7. The product receiver is as close as possible to the product end of the columns to minimize pressure drops between the units. This is necessary to ensure that the columns during high pressure feed differ in pressure only because of pressure drop in the bed. This minimizes any pressurization of the beds by the feed gas.
8. The gas heat exchanger to cool the product is simply a 1/2 in. O.D. x 35 ft. long copper tube.

b. Procedure

1. Cycle time selection - To operate the process with constant feed rate it is necessary to satisfy the following equation:

$$t_H = t_L + t_{BD} + t_{PR}$$

Since breakthrough experiments are accurate, t_H can be predicted from the theory or simply measured for a given feed rate. t_{BD} and t_{PR} are dependent upon how the system is constructed (i.e. L/D of columns, fittings...). t_{BD} can be determined experimentally by simply monitoring pressure-vs-time during a blowdown step. Analogously, t_{PR} can be measured experimentally. It is important to minimize

$t_{BD} + t_{PR}$ so t_L is as large as possible. This allows the purge flow rate to be as small as possible resulting in minimal pressure drop during the purge step.

For a given feed rate, feed pressure, pressure ratio, and available time for purge, t_L , the required molar purge rate is known. With the product receiver at the desired operating temperature and pressure containing light product, metering valves MV2 and MV3 are tuned "identically" to the desired purge flow by connecting a wet test meter to the two-way valves TV1 and TV2. The process is ready for operation as cycle times have been defined and the purge valves (MV2 and MV3) are set.

2. Conservative Start-Up - It is implicitly assumed that the theory is accurate in the cycle time selection. To avoid bias the process is started up under conservative conditions. That is, the desired feed rate used to calculate t_H is reduced but t_H is kept the same. With this approach the composition shock does not reach the end of the bed during the feed step. Additionally, the pressure of the blowdown and purge steps is reduced below the value used to set purge valves. This ensures that the purge is adequate to thoroughly remove the heavy component.

Prior to start-up the process is purged with light component. In addition it is pressurized to the design

conditions. The entire process is heated to the desired temperature. The solenoid valves can now be activated by the computer with the appropriate cycle times and the process operated.

3. Tuning the Process - For the conditions of the conservative start-up a pure product is produced but the recovery is not the maximum. In fact, if the pressure ratio is quite low and the start-up overly conservative then system pressure will drop even with MV4 closed. This is a negative recovery problem. As Figure 14 indicates, negative recovery can occur even with optimum (nonconservative) settings.

Assuming that the start-up is not overly conservative and the pressure ratio is great enough to ensure positive recovery the process can be tuned. First, the feed rate is slowly increased until heavy component appears in the product. The feed rate is operated at a valve just below the valve that results in heavy component in the product. The composition shock is allowed to reach the end of the column but not exit it. Second, the low pressure step is slowly increased to higher pressures (by opening MV5) until heavy component appears in the product. The operating low pressure uses the minimal amount of purge flow. That is, the composition simple-wave reaches the feed end of the bed but does not exit.

During the tuning steps above the product valve MV4 is adjusted to ensure that the pressure in the product receiver is maintained at the desired level. Finally, MV4 is set to ensure that the cycle to cycle pressure is constant.

4. Attaining Steady State - After the procedural steps above are completed the process is operated without process changes for several hours (often overnight) to ensure steady state conditions are attained. This is required because of the slow dynamics induced by the large volume product receiver. Once steady state is reached data is taken each hour for up to six hours.
5. New Conditions - When a different condition is studied steps 1 through 4 are repeated if necessary. At 45°C, for example, a variety of pressure ratios are studied so it is only necessary to change the pressure of the blowdown and purge steps and the purge valve (MV2 and MV3) positions.

c. Data and Calculations

1. Theory

$$R_{TH} = (1 - \beta) \left(1 - \frac{1}{\rho(1 - Y_F)} \right)$$

$$\beta = 0.59293, \quad Y_F = .7826$$

$$R_{TH} = 0.40707 - \frac{1.87245}{\rho} \quad (\text{at } 45^\circ\text{C})$$

2. Experiment

Run 1: Five data points collected at half hour intervals
for two hours.

$$\overline{P}_H = 44.753 \text{ psia} \pm 0.07\%$$

$$\overline{\Delta P}_H = 0.674 \text{ psi} \pm 2.7\%$$

$$\overline{P}_L = 6.911 \text{ psia} \pm 0.03\%$$

$$\overline{\Delta P}_L = 0.596 \text{ psi} \pm 0.62\%$$

$$\overline{\rho} = 6.476$$

$$\overline{(1-\gamma_E)} = .9972 \pm 0.01\%$$

$$\overline{F}_B = 0.5598 \text{ l/m} \pm 0.00\%$$

$$\overline{E}_B = 0.0570 \text{ l/m} \pm 2.7\%$$

$$\overline{R}_{EXP} = 0.10174 \pm 2.7\%$$

$$\overline{R}_{TH} = 0.1179$$

] at 747 mmHg
22°C

Comment: Bed temperature varies from 40.5°C to
47.8°C during a cycle. Cycle times given
in Table 6.

Run 2: Five data points collected over a three hour
period.

$$\overline{P}_H = 45.464 \text{ psia} \pm 0.05\%$$

$$\overline{\Delta P}_H = 0.632 \text{ psi} \pm 3.8\%$$

$$\overline{P}_L = 5.9085 \text{ psia} \pm 0.01\%$$

$$\overline{\Delta P}_L = 0.5244 \text{ psi} \pm 0.26\%$$

$$\overline{\rho} = 7.695$$

$$\overline{(1-\gamma_E)} = .9974 \pm 0.01\%$$

$$\begin{aligned}\overline{F}_B &= 0.5596 \text{ l/m} \pm 0.3\% \\ \overline{E}_B &= 0.1025 \text{ l/m} \pm 2.0\% \\ \overline{R}_{EXP} &= 0.1838 \pm 1.6\% \\ \overline{R}_{TH} &= 0.1637_3\end{aligned}$$

Comment: Bed temperature varies from 40.5°C to 47.8°C . Cycle times given in Table 6.

Run 3: Five data points collected a half hour intervals for two hours.

$$\begin{aligned}\overline{P}_H &= 45.297 \text{ psia} \pm 0.03\% \\ \overline{\Delta P}_H &= 0.632 \text{ psi} \pm 1.32\% \\ \overline{P}_L &= 3.664 \text{ psia} \pm 0.01\% \\ \overline{\Delta P}_L &= 0.4836 \text{ psi} \pm 0.00\% \\ \overline{P} &= 12.363 \\ \overline{(1-Y_E)} &= 0.9975 \pm 0.04\% \\ \overline{F}_B &= 0.5576 \text{ l/m} \pm 0.4\% \\ \overline{E}_B &= 0.1606 \text{ l/m} \pm 2.7\% \\ \overline{R}_{EXP} &= 0.2870 \pm 2.9\% \\ \overline{R}_{TH} &= 0.2556\end{aligned}$$

Comment: Bed temperature varies from 41.1°C to 48.3°C . Cycle times given in Table 6.

Run 4: Seven data points collected over a five hour period.

$$\begin{aligned}\overline{P}_H &= 43.946 \text{ psia} \pm 0.38\% \\ \overline{\Delta P}_H &= 0.674 \text{ psi} \pm 18.4\% \\ \overline{P}_L &= 1.867 \text{ psia} \pm 1.2\%\end{aligned}$$

$$\begin{aligned}
 \overline{\Delta P_L} &= 0.491 \text{ psi} \pm 1.7\% \\
 \overline{\rho} &= 23.538 \\
 \overline{(1-Y_E)} &= 0.9980 \pm 0.04\% \\
 \overline{F_B} &= 0.5531 1/m \pm 0.8\% \quad] \text{ at } 747 \text{ mmHg} \\
 \overline{E_B} &= 0.1822 1/m \pm 1.2\% \quad] 22^\circ\text{C} \\
 \overline{R_{EXP}} &= 0.3294 \pm 0.8\% \\
 \overline{R_{TH}} &= 0.3275
 \end{aligned}$$

Comment: Bed temperature varies from 40.0°C to 47.8°C . Cycle times given in Table 6.

Run 5: Four data point collected over a two hour period.

$$\begin{aligned}
 \overline{P_H} &= 46.60 \text{ psia} \pm 0.08\% \\
 \overline{\Delta P_H} &= 0.550 \text{ psi} \pm 7.4\% \\
 \overline{P_L} &= 3.0 \text{ mm Hg} \\
 \overline{\Delta P_L} &= ---- \\
 \overline{\rho} &= 803 \\
 \overline{(1-Y_E)} &= .9927 \pm 0.026\% \\
 \overline{F_B} &= 0.5603 1/m \pm 0.16\% \quad] \text{ at } 747 \text{ mmHg} \\
 \overline{E_B} &= 0.2278 1/m \pm 1.52\% \quad] 22^\circ\text{C} \\
 \overline{R_{EXP}} &= 0.4067 \pm 1.5\% \\
 \overline{R_{TH}} &= 0.4047
 \end{aligned}$$

Comment: Bed temperature varies from 41.1°C to 48.9°C during a cycle.

Cycle Times

Step	Valves Open	Time Open (sec)
1	2, 4, 7	100
2	2, 7, 8	5
3	1, 3, 8	100
4	3, 7, 8	5

Run 6: Four data points collected over two and one-half hours.

$$\overline{P_H} = 43.85 \text{ psia} \pm 0.08\%$$

$$\overline{\Delta P_H} = 0.645 \text{ psi} \pm 5.1\%$$

$$\overline{P_L} = 2.7 \text{ mmHg}$$

$$\overline{\Delta P_L} = \text{----}$$

$$\rho = 840$$

$$\overline{(1-Y_E)} = .9934$$

$$\overline{F_B} = 0.4424 \text{ l/m} \pm 0.5\% \quad] \text{ at } 747 \text{ mmHg}$$

$$\overline{E_B} = 0.1917 \text{ l/m} \pm 3.1\% \quad] 22^\circ\text{C}$$

$$\overline{R_{EXP}} = 0.4332 \pm 3\%$$

$$\overline{R_{TH}} = 0.4492$$

Comment: Bed temperature varies from 57.2°C to 62.8°C during a cycle.

Cycle Times

Step	Valves Open	Time Open (sec)
1	2, 4, 7	100
2	2, 7, 8	5
3	1, 3, 8	100
4	3, 7, 8	5

Comment: To calculate the pressure ratio it is necessary to evaluate P_H at the end of step 3 (see Figure 12). In this study, however, a complete set of data for P_H at the end of step 3 was not collected. Complete P_H data was collected at the end of step 2. Therefore, for the sake of consistency, all calculations of the pressure ratio are performed using P_H at the end of step 2. The differences are quite small since P_H (step 2) is only about 2% greater than P_H (step 3). The net effect on the recovery data is a slight shift of the data to higher than actual pressure ratios. A correction would not cause an increase in the average absolute difference between experiment and theory.

F. Equipment Summary

1. The temperature sensors and indicating units are denoted at TI. Omega Type-K thermocouples and associated indicating units are employed in all experiments. The tips of the thermocouples are removed exposing the wire junction to the process stream thus facilitating faster temperature monitoring response.

Omega Eng. Inc., Stamford, CT.
2. The pressure indicating (PI) gauges are Wallace-Tiernan High Accuracy Gauge Line type. 0-150 psia gauges are used at positions where pressures above atmospheric are monitored while 0-800 mmHg gauges are employed at atmospheric pressures and below.

Wallace & Tiernan, Belleville, N.J.
3. The pressure transducing (PT) and delta-pressure transducing (PT) units are identical and consist of Validyne pressure transducers and Validyne CD12 indicators (0-10 V output).

Validyne Engineering, Northridge, CA.
4. Composition monitoring is performed using either a Perkin-Elmer mass spectrometer (MGA-100) or a Beckman oxygen analyzer (OM-11). The mass spectrometer is used in all PSA experiments and N₂(A)-O₂(B) breakthrough measurements. The

oxygen analyzer is used in the O₂(A)-Ar(B) breakthrough experiments since the mass spectrometer can only handle argon compositions under 5%_{vol.}.

Perkin-Elmer, Norwalk, CT.

Beckman Instruments Inc., Fullerton, CA.

5. Flow measurements are performed primarily by wet test meter and hot wire anemometer. The wet test meter is a precision scientific unit while the hot wire anemometer is a Technology Inc. Model LFC-6. The wet test meter is calibrated and used to calibrate the LFC-6 unit to obtain a voltage-vs-mass flow curve.

Technology Inc., Dayton, OH.

6. The solenoid valves are 1/4" orifice, 40 psi. M.O.P.D., stainless steel.

Allied Inc., Wilmington, OH.

7. The solenoid valves are computer controlled by a Digital Declarab 11/03 minicomputer.

Digital Equipment Corp., Marlboro, Mass.

8. A Gould, 4-pen, BRUSH-model strip chart recorder is used in breakthrough experiments and PSA process monitoring.

Gould Inc., Cleveland, OH.